AD-A104 453 UNIVERSITY OF CENTRAL FLORIDA ORLANDO ENGINEERING AN--ETC F/G 20/5
LASER MARKSMANSHIP EVALUATION: A UNIVERSAL MATH MODEL AND EXPER--ETC(U)
NOV 80 R L PHILLIPS, L C ANDREWS N61339-79-D-0105

UNCLASSIFIED PM-TRADE-RE-0008-81 NL

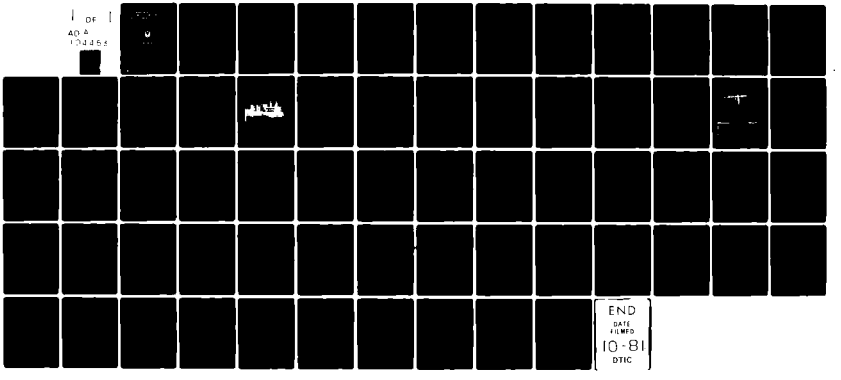

END
DATE FILMED
10-81
DTIC

LEVEL II

LASER MARKSMANSHIP EVALUATION: A UNIVERSAL MATH MODEL AND EXPERIMENTAL VERIFICATION

by
Ronald L. Phillips
Larry C. Andrews

FINAL REPORT

PREPARED FOR

U.S. ARMY PROJECT MANAGER FOR TRAINING DEVICES
located at
NAVAL TRAINING EQUIPMENT CENTER (NTEC)
ORLANDO, FLORIDA 32813

by

ENGINEERING AND INDUSTRIAL EXPERIMENT STATION
COLLEGE OF ENGINEERING
UNIVERSITY OF CENTRAL FLORIDA

NOVEMBER 1980

DISCLAIMER

The contents of this publication are not to be construed as an official Department of the Army position, unless so designated by other authorized documents.

Citation of manufacturer's or trade names does not institute an official endorsement or approval of the use thereof.

Destroy this report when no longer needed. Do not return it to the originator.

Unclassified

SECURITY CLASSIFICATION OF THIS PAGE (When Data Entered)

REPORT DOCUMENTATION PAGE	READ INSTRUCTIONS BEFORE COMPLETING FORM
1 REPORT NUMBER: PMT-RE-0008-81	2 GOVT ACCESSION NO: AD-A104 453
	3 RECIPIENT'S CATALOG NUMBER
4 TITLE (and Subtitle): Laser Marksmanship Evaluation: A Universal Math Model and Experimental Verification	5 TYPE OF REPORT & PERIOD COVERED: Final Report
	6 PERFORMING ORG. REPORT NUMBER
7 AUTHOR(s): R. L. Phillips and L. C. Andrews	8 CONTRACT OR GRANT NUMBER(s): N61339-79-D-0105 DO 0027
9 PERFORMING ORGANIZATION NAME AND ADDRESS: Engineering & Industrial Experiment Station, University of Central Florida, P.O. Box 25000, Orlando 32816	10 PROGRAM ELEMENT, PROJECT, TASK AREA & WORK UNIT NUMBERS: 62727A230
11 CONTROLLING OFFICE NAME AND ADDRESS: Research and Engineering Management Div., PM TRADE, Principal Investigator A. Boudreaux 305-646-5771	12 REPORT DATE: November 1980
	13 NUMBER OF PAGES: 56
14 MONITORING AGENCY NAME & ADDRESS (if different from Controlling Office): Project Manager for Training Devices, United States Army, Orlando, FL 32813	15 SECURITY CLASS (of this report): Unclassified
	15a DECLASSIFICATION DOWNGRADING SCHEDULE

16 DISTRIBUTION STATEMENT (of this Report)

Approved for public release; distribution unlimited.

17 DISTRIBUTION STATEMENT (of the abstract entered in Block 20, if different from Report)

18 SUPPLEMENTARY NOTES

19 KEY WORDS (Continue on reverse side if necessary and identify by block number)

Training device technology
MILES
Laser propagation
Marksmanship
Atmospheric turbulence
Optical communications

20 ABSTRACT (Continue on reverse side if necessary and identify by block number)

The MILES 105 mm main tank gun transmitter was tested for the potential of using the system as a marksmanship trainer. The tests were carried out over a 3000 meter range at the Space Shuttle runway at Kennedy Space Center. Experimental evidence collected in CW laser experiments show that the statistical distribution used in the MILES development, i.e., Log-Normal, is valid only over short ranges. At long ranges the Negative Exponential

DD FORM 1 JAN 73 1473 EDITION OF 1 NOV 65 IS OBSOLETE
S/N 0102-014-6601

Unclassified

SECURITY CLASSIFICATION OF THIS PAGE (When Data Entered)

20. Abstract (cont'd)

distribution was measured. A new universal math model was developed which accurately described the statistics of the fluctuation laser signal along the entire range up to 3000 meters. Using this new universal model the cummulative fading was calculated. This analysis showed that it is the intermediate ranges which have the greatest fading. Based upon the experimental evidence and the math model we conclude that the MILES system is not sufficiently accurate for long range gunnery marksmanship training, but that a new CW laser transmitter and receiver, developed by NTEC in a parallel project, should meet the required accuracy.

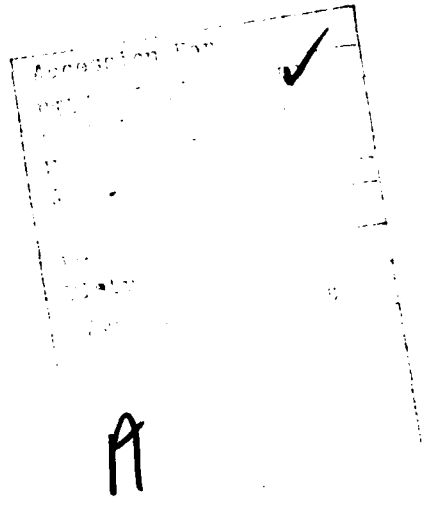

A

ACKNOWLEDGEMENT

The authors wish to thank Mr. Madjid Belkerdid, Mr. Sunder Gopani, and Miss Linda Coulter who all worked long hours on this project. We are also indebted to Mr. Billie L. Study, Manager of the Space Shuttle Landing Facility, for his cooperation and help during these experiments at Kennedy Space Center.

SUMMARY

This document reports on a research project directed by PM TRADE and performed jointly by the Engineering and Industrial Experiment Station of the University of Central Florida (UCF) and the Research Department of the Naval Training Equipment Center (NTEC). The project centered on the study of the use of the MILES system as a marksmanship trainer for long-range tank and anti-tank gunnery.

The study evaluated the MILES 105mm laser transmitter with the MILES 105mm standard target. During the tests the atmospheric optical channel was simultaneously monitored by a CW laser propagating parallel to MILES 105mm beam. The test results show the MILES beam is much wider than predicted by the analysis in the document MILES A002, June 1980. Also a comparison of the UCF and the NTEC test results show that the background sun illumination significantly reduces the effective range.

The study also evaluated the statistical model (Log-Normal distribution) used as a basis of the MILES design and for prediction of its operational characteristic. The evidence collected during experiments conducted at the Space Shuttle runway at Kennedy Space Center shows that the Log-Normal distribution was valid only up to ranges of about 180 meters. At long ranges, under conditions of strong atmospheric turbulence, the Negative Exponential distribution was measured. The UCF team developed a universal math model which agreed with both the distribution at the short and long ranges as well as the measured distribution at intermediate ranges. The cumulative fade was then calculated from the universal math model. The results show that the intermediate ranges have the largest fading.

The recommendations for MILES add-ons are: to replace the MILES detectors with photo-diodes, to replace the transmitter with a high pulse rate CW laser diode transmitter, and to replace the receiver with a corresponding phase locked loop or matched filter receiver. These systems could be made completely compatible with the MILES encoder and decoder. The threshold of this receiver and the pulse rate can be set by analysis of the UCF universal math model for the laser propagation communication channel. The study's results support the conclusion that the current MILES system is not sufficiently accurate to be used as a marksmanship gunnery trainer. The analysis supports the contention that the required accuracy can be obtained by using a high pulse rate CW laser diode transmitter and the appropriate CW receiver as proposed by the NTEC research team.

The PM TRADE project director was A. J. Boudreaux. The NTEC research team leader was A. H. Marshall, and the UCF team head was R. L. Phillips.

TABLE OF CONTENTS

LIST OF ILLUSTRATIONS

SECTION I

INTRODUCTION

This document reports on a project which undertook the evaluation of the MILES system as a long-range marksmanship gunnery trainer. The project consisted of measurements on a MILES tank main gun transmitter, analysis of the mathematical models of the laser propagation, analysis of the MILES receiver binary union decoder, and the development of a new CW laser transmitter and receiver which could be used as an add-on for marksmanship uses of MILES. The project was organized in two research teams. The University of Central Florida (UCF) team performed the mathematical analysis and the experimental verification of the mathematical models of the laser propagation phenomenon upon which much of the MILES system design is based. The Research Department of the Naval Training Equipment Center (NTEC) conducted the development of the CW laser transmitter and receiver hardware. In addition both teams took extensive measurements on the MILES tank main gun simulator.

The MILES system was designed and constructed as a short range tactical laser weapon fire simulator. It was designed not to simulate the flight of a particular round, but rather, to simulate the probability of a kill in an engagement. The "MILES kill" may occur because of a successful detection and decode of a MILES code word by any of the MILES detectors on the target. To ensure kills in a tactical engagement, the transmitted laser beam was made sufficiently wide to make the kill zone actually wider than the target. In other words, the weapon can be aimed at a point actually off the target and a kill could still be obtained.

If MILES is to be used in gunnery marksmanship training, a much smaller and well-defined kill zone will be required. The kill zone is defined by an inter-play between the transmitter and receiver characteristics, but it is the receiver structure which has the dominant effect. The basic receiver can be divided into three portions — the detector, the receiver, and the decoder which is used to decipher the MILES codes. The mathematical model used to describe the laser atmospheric channel which served as a basis for their design and performance evaluation of the decoder and the codes, was the Log-Normal statistic. If any MILES add-ons were to be designed, the validity of this model would require testing. Some of the experiments carried out to investigate the statistics of long-range laser propagation were described in a previous report [1]. Those experiments were augmented by further experiments conducted in August 1980 at Kennedy Space Center Shuttle Landing Facility. The results of those investigations are reported in Section III of this document.

The essence of the long-range detection and decoding problem is the determination of transmitted MILES code from a random-fading received signal in the midst of receiver noise. Two techniques widely used in communication systems to extract a fading signal in the presence of noise are phase-locked loops and matched active filters. These two approaches were investigated by the research team at NTEC. Both of these receiver types require a CW laser transmitter operating at a high pulse rate. The required detector for both of these techniques is a high speed device such as a reversed biased photo-diode or photo-avalanche diode. The parameters that must be determined, for either the phase-locked loop or the matched-active filter, are the receiver

threshold and the transmitter pulse repetition frequency (PRF). If these systems are to be compatible with the MILES encoder and decoder, the systems must operate at a multiple of the MILES PRF of 3 KHz. For instance, if twenty pulses were required by the receiver to acquire the signal, the necessary PRF would be 60 KHz. Then every time the MILES encoder commanded the transmitter to send a pulse, corresponding to a MILES code "one", the CW transmitter would transmit twenty pulses during the same period. The detector would then detect the signal and the receiver would lock onto the twenty pulses and then pass a single pulse onto the MILES decoder at the MILES PRF of 3 KHz. Hence the new CW laser transmitter and detector/receiver would be "invisible" to the MILES encoder and decoder.

So as to determine the best PRF for the transmitter, the optimum receiver threshold and the required transmitter beam width, a mathematical model is required to accurately predict the statistical scattering of the atmosphere. The required models are the probability density function, the cummulative fading, and the average fade period length. The models must be universally accurate at all extended ranges if the system is to simulate the flight of a particular round as required in marksmanship gunnery training.

Section II reports on the measurements made on the MILES main tank gun simulator. The atmospheric turbulence conditions and the background sun were simultaneously monitored and their effects on the MILES simulator are discussed.

Section III develops the universal mathematical model for laser beam propagation over ranges up to 3 Km. This section also discusses the fading time of the scattered laser signal.

SECTION II

MEASUREMENTS OF THE MILES SYSTEM

Measurements were made on a MILES 105 mm tank main gun laser transmitter and an armored personnel carrier (APC) receiver system. Data was taken on the system on a darkened indoor range and on a long outdoor range.

EXPERIMENTAL LAYOUT

The indoor tests were made at a range of exactly 100 feet in complete darkness. The MILES 105 mm transmitter was rigidly mounted on a tripod one meter above the floor. The target was the MILES APC receiver using only one detector. The other detectors were all taped to prevent any light leak whatsoever. Initially, the transmitter was aimed directly at the detector and then moved off center both horizontally and vertically in one-inch steps. At each position the transmitter was fired ten times. If all ten shots were kills, the transmitter aim point was moved another inch away from the detector. When one miss was recorded, the location was noted. The transmitter aim point was moved in each of the four directions off of the detector as shown in Figure 2-1. These measurements then established the divergence of the 90% kill zone in the near field of the transmitter.

The long-range tests were carried out at the Space Shuttle runway at NASA's Kennedy Space Center. The runway is 16,000 feet long and 150 feet wide and completely level. It is constructed of concrete with grooves cut across it every inch for the entire length. Hence, the

exact range over which the tests were made was measured very accurately. The area around the runway was cleared of all structures and all vegetation, except grass, for distances of several hundred feet. These features of the runway allowed the MILES tests to be conducted over a completely homogeneous range ensuring the test results would be repeatable. A schematic of the Space Shuttle runway is shown in Figure 2-2.

The MILES 105 mm laser transmitter was mounted on an optical rail along side of a HeNe (wavelength 0.6328 mm) CW laser also mounted on an optical rail. The two rails were then attached to the head of a tripod which could be rotated both in the horizontal and vertical planes with an accuracy of an arc minute. The lasers were pointed down the length of the runway at a height of 1.3 meters above and level with the surface.

The MILES APC receiver belt system was mounted on a standard MILES 105 mm target as described in the Xerox CDRL Item A002, Trainer Engineering Report for MILES Volume I, June 4, 1980. The APC receiver belt was attached to the target with five of the six detectors facing up range, and the sixth detector completely taped as prescribed in Xerox A002. The entire target was then mounted vertically on the side of a van at a height of three feet above the runway surface. The target mounted on the van is shown in Figure 2-3. The target was moved in one-half meter increments across the MILES 105 mm transmitter beam and at each new position ten shots were fired. This procedure was repeated until one shot was missed out of ten shots fired. These measurements were performed across the beam thereby defining the 90% kill zone of the beam at that range. The measurements were taken at

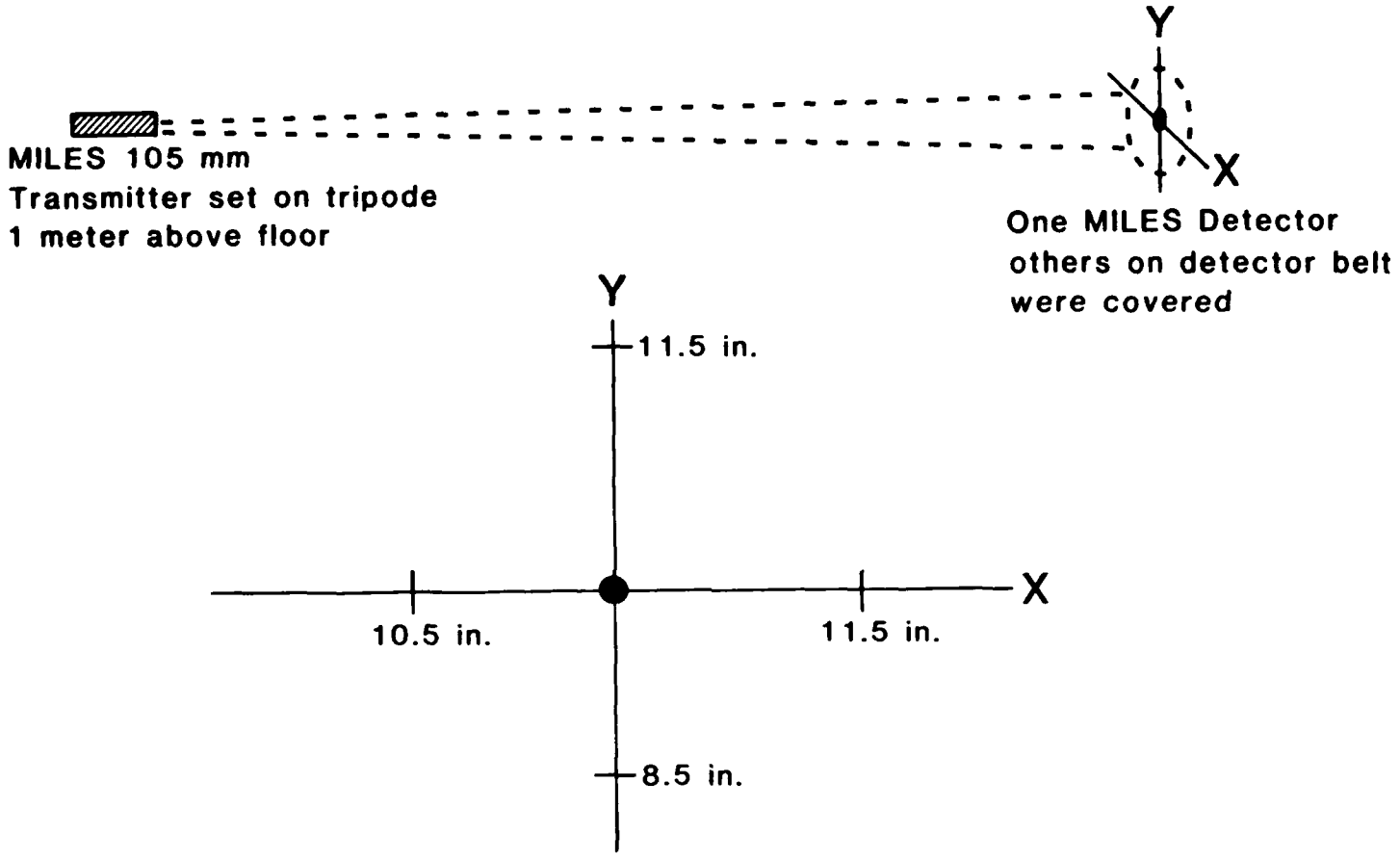

Fig. 2-1. Kill zone of 90% for a single detector at 100 feet for a completely dark indoor range.

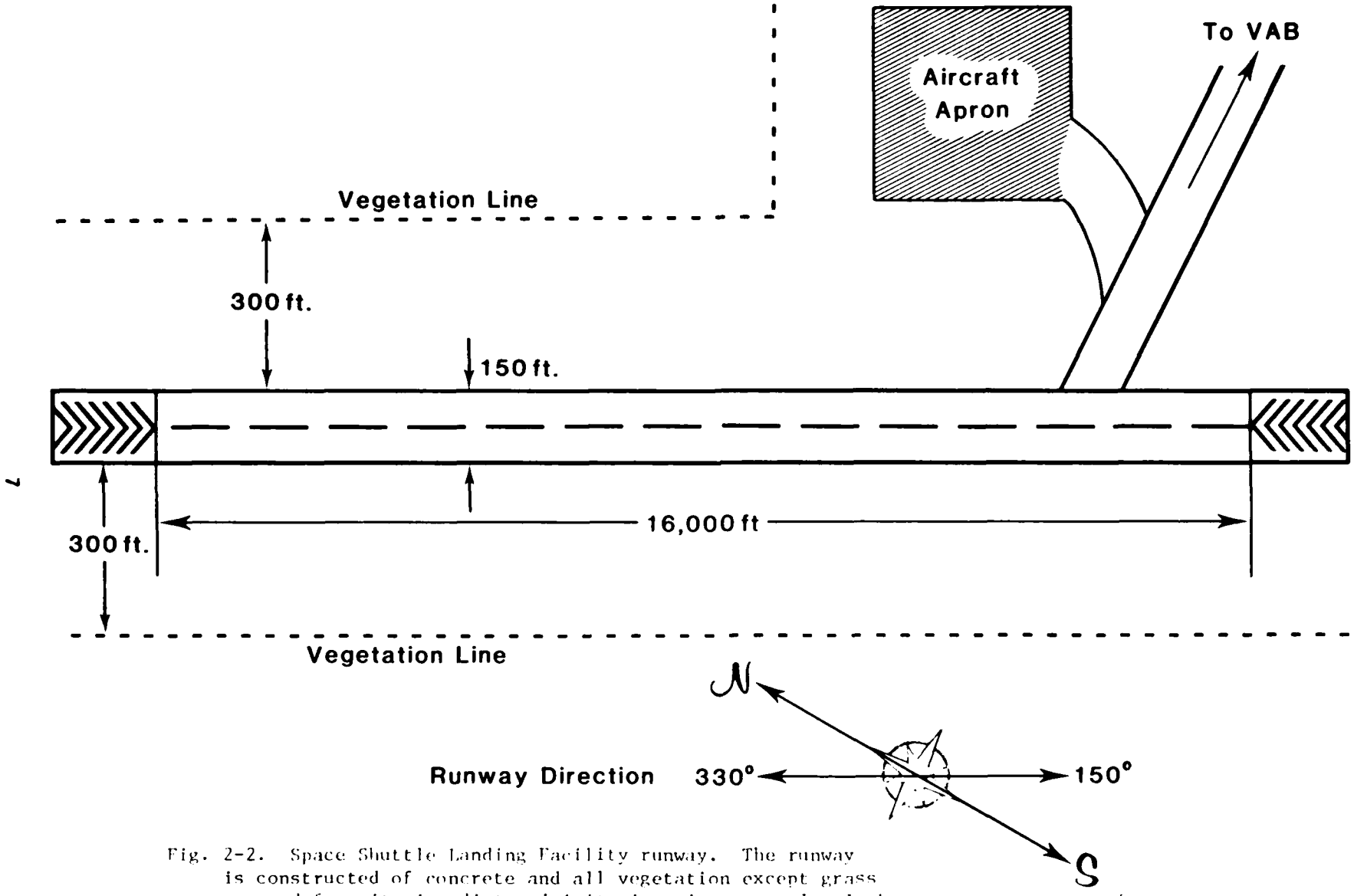

Fig. 2-2. Space Shuttle Landing Facility runway. The runway is constructed of concrete and all vegetation except grass removed from its immediate vicinity insuring a completely homogeneous atmospheric optical channel.

Fig. 2-3. MILES target mounted on side of van during testing of the 105 mm transmitter. The truck in the background housed the long range CW laser receiver used to monitor the optical channel.

500 meter increments starting at 500 meters and continuing down range to 3000 meters.

During the MILES measurements, the background solar illumination was monitored. Also monitored were the temperature, wind speed, and wind direction.

The CW laser system parallel to the MILES beam allowed for simultaneous measurements of the atmospheric channel through which the MILES signal was being transmitted. The CW laser signal was measured at a short-range station and at a long-range station. The short-range station was located at a fixed position 183 meters from the transmitter. At this station special electronics sampled the CW laser beam every minute and calculated the average signal level and the variance of the CW laser signal fluctuations induced by atmospheric turbulence. The long-range station was always located down range at the same position as the MILES receiver target. The laser signal was monitored at this station by a MINC-11 computer built by Digital Equipment Corporation. The MINC-11 computer calculated the first five statistical moments of the fluctuating CW laser signal. Before the tests of the MILES system began, the long-range station was placed alongside of the short-range station. Using the first five statistical moments, it was established that at 183 meters from the transmitter the short-range station would be located within the range for which the Log-Normal mathematical model for the laser scattering would be valid. In this regime only the mean value and the variance of the fluctuating signal are needed to calculate the so-called atmospheric turbulence structure constant, C_n^2. This constant is the measure of the strength of the atmospheric turbulence,

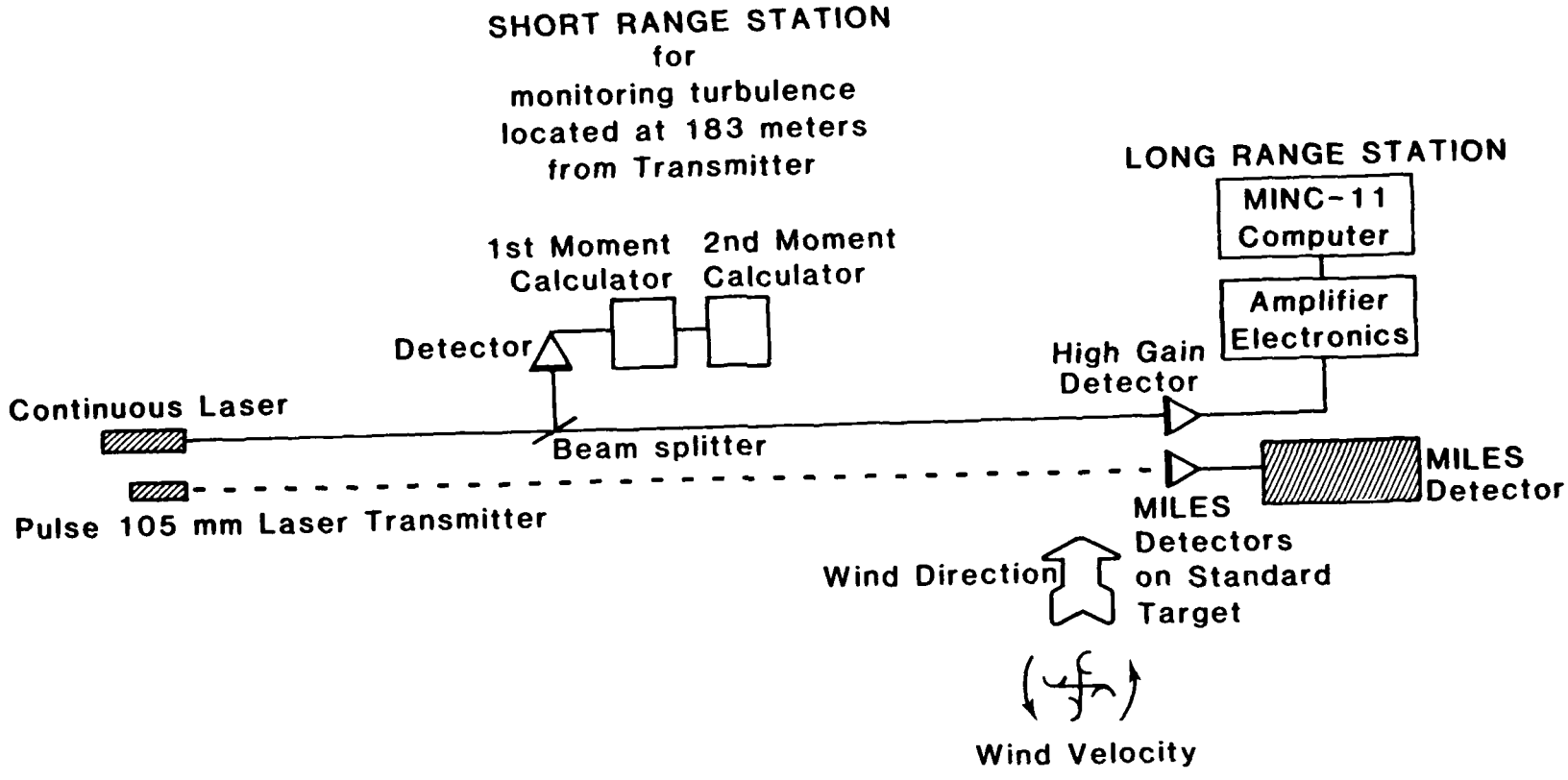

Fig. 2-4. Experimental layout of long range and short range stations on outdoor range at the Space Shuttle runway at Kennedy Space Center.

where:

turbulence		$C_n^2\ m^{-2/3}$
weak	$\leq$	10^{-15}
moderate	$\simeq$	10^{-14}
strong	$\geq$	10^{-12}

Hence using the data from the short-range station, the strength of the turbulence present in the optical channel can be calculated. The homogeneity of the Shuttle runway assured the measured C_n^2 at the short-range station was valid for the entire range. The statistical moments from the long-range station along with the data from the short-range station allowed for the complete characterization of the scattering statistics of the CW laser channel and thereby the statistics of the parallel MILES laser communication channel. The experimental layout of the tests at the Space Shuttle runway are shown in Figure 2-4.

RESULTS

The 90% kill zone for the short-range indoor tests is shown in Figure 2-1. The near field 90% kill zone has an effective horizontal divergence of 20 milliradians and a vertical divergence of 14 milliradians at 100 feet.

The long-range outdoor measurements of the 90% kill zone is shown in Figure 2-5. The dotted curve shows the predicted 90% kill zone as depicted in Figure F-16, page F-34, of Xerox A002, Volume I, June 4, 1980. The Xerox curve used for comparison was the 50 Km visibility curve since there were unlimited visibility conditions during the MILES

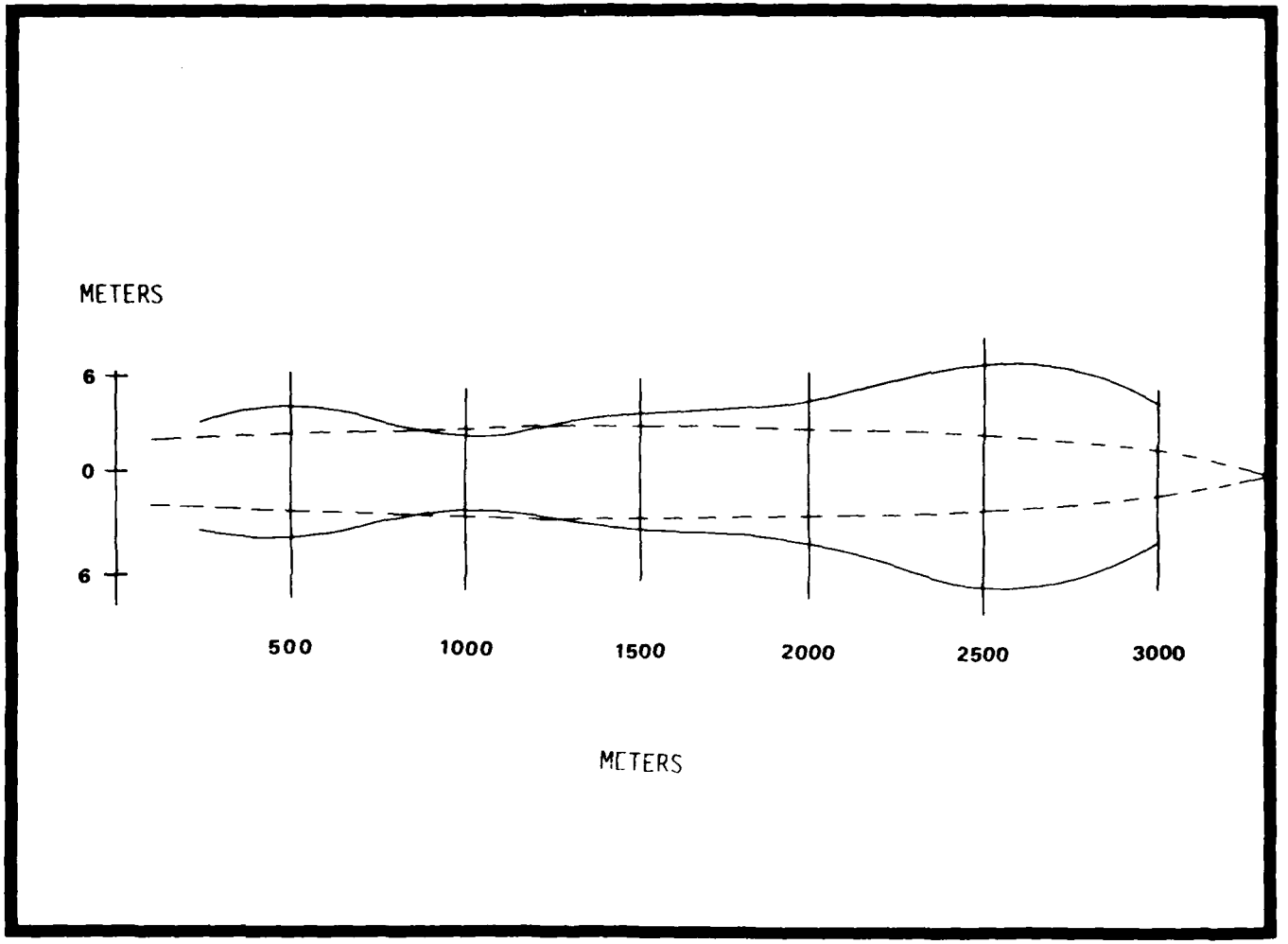

Fig. 2-5. The solid curve shows the 90% probability curve for the 105 mm transmitter as measured at the Shuttle runway. Measurements were made only out to 3000 meters but the data shows that the 90% kill zone actually extends slightly further. The dotted curve is the theoretically predicted curve from the Xerox A002 document.

tests at the Shuttle runway. The turbulence structure constant C_n^2 varied only slightly from 10^{-11} $m^{-2/3}$ to 10^{-13} $m^{-2/3}$ which means the turbulence remained very strong. The C_n^2 was calculated using the equation

$$C_n^2 = \frac{Ln\ (\langle I^2 \rangle / \langle I \rangle^2)}{0.5\ K^{7/6}\ L^{11/6}} \qquad (2.1)$$

where $\langle I^2 \rangle / \langle I \rangle^2$ is the normalized second moment obtained from the measurements of $\langle I^2 \rangle$, and $\langle I \rangle$ at the short range station for the CW laser beam, $K = 2\pi/\lambda$ (λ is the wavelength), and L is the range (183 meters).

During the tests on the MILES system the background sunlight was monitored. The background measurements were made with a 40X OPTO-METER from United Detector Technology Inc. The device was calibrated in lumens/square foot or footcandles. Typically, the sun illuminance on the MILES target varied from 10^3 to $7x10^3$ lumens/square foot. The variation was due to the cloud movements in the partially overcast sky. The partially overcast sky and the fact that the target was facing almost south (150° from north) meant that very little of the direct sunlight was incident on the target. This should be contrasted with the experimental layout of the MILES tests conducted by NTEC. In those tests the MILES receiver belt faced almost due west [2]. Since those long-range tests were conducted later in the day, the full sun shown directly onto the target.

The effect of background sunlight on the MILES unbiased solar cell can be severe. The effects of background illumination has been studied in an earlier publication of Mallette and Phillips. A reprint of that

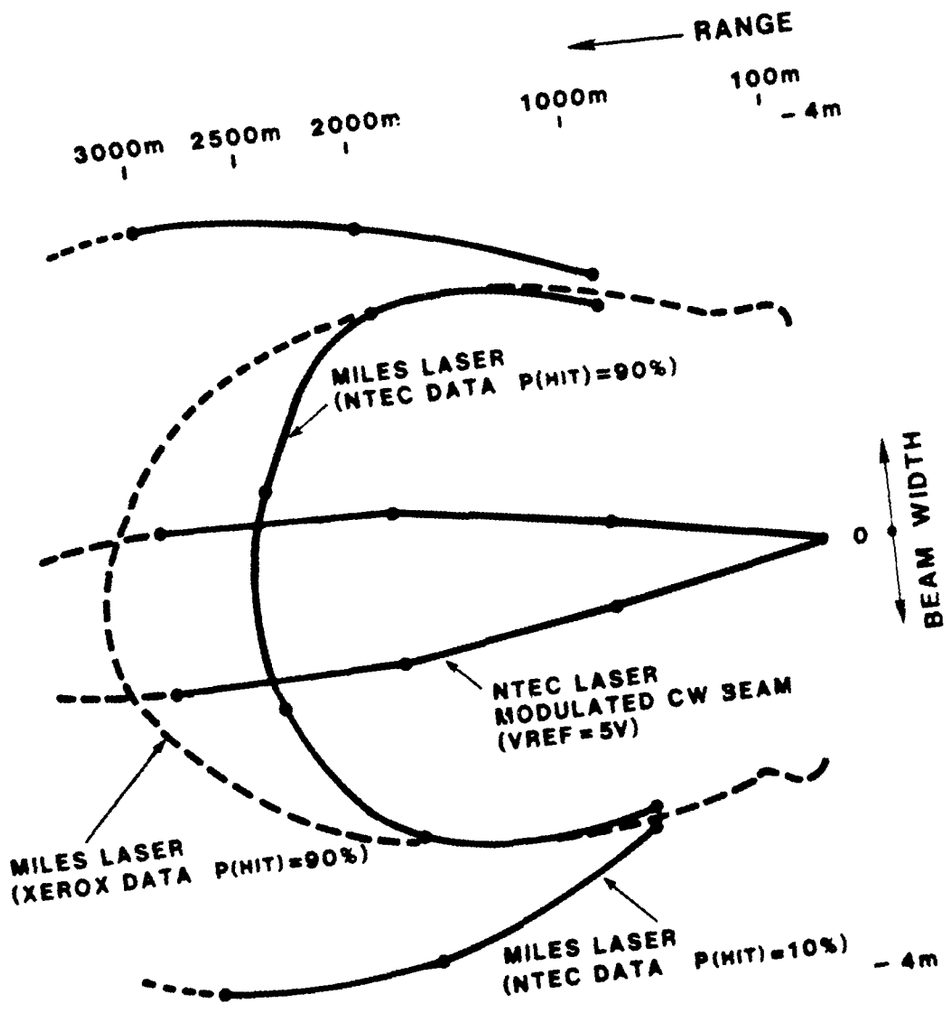

Fig. 2-6. MILES 90% kill zone as measured by NTEC [2]. The 90% curve measured by NTEC shows a significantly shorter range than measured by UCF.

publication is enclosed in Appendix D. The effects of temperature on the MILES detector has also been explored and reported in Reference [6]. The effect of high temperature and especially background illumination is to reduce the sensitivity of the detector. It is this reduced sensitivity, due to the greater sun background light, which caused the NTEC tests to show an effective 90% kill range of only 2,500 meters while the UCF tests at Kennedy Space Center show an effective 90% range of over 3,000 meters as shown in Figure 2-5. The NTEC experimental results are shown in Figure 2-6, for comparison.

The UCF measured 90% beam width shows several "bulges" in the beam. These "bulges" seem to be due to the tri-gaussian nature of the transmitter beam as described in Xerox A002. The evidence to support this is that the first "bulge" correspnds to the 90% kill zone divergence as measured on the 100-foot range. The second bulge occurring at about 1,500 meters is not as pronounced as the first due to the natural beam spreading. The "bulge" at the longest range corresponds to the third gaussian component of the tri-gaussian beam.

DISCUSSION

The data taken in the tests at Kennedy Space Center showed a much greater range and wider kill zone for the MILES system than did the NTEC test results. This is due to the much lower background sun illumination of the MILES detectors in the UCF tests.

The UCF tests showed that the beam width varies along the range. This was due to the inherent shape of the laser diode output beam in the MILES transmitter. The beam width shows three bulges characteristic of a tri-gaussian beam shape.

(a)

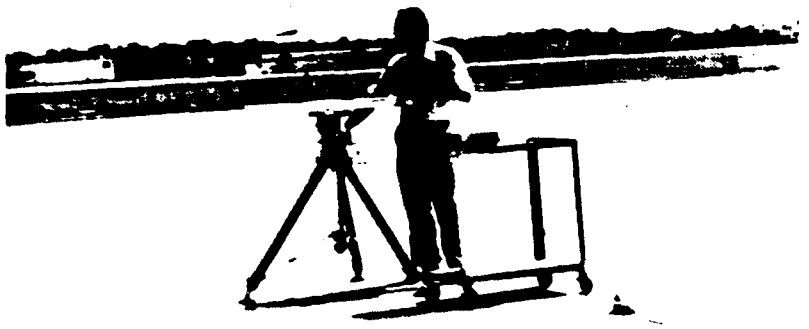

(b)

Fig. 2-7. (a). CW laser transmitter used to monitor atmospheric optical channel during MILES test. (b). CW laser as seen from down range from MILES target location.

SECTION III

UNIVERSAL MODEL FOR TURBULENCE LASER SCATTERING

An accurate universal (valid at all ranges) mathematical model is a stronger requirement for marksmanship training than for tactical training due to the small well defined kill zone needed for the marksmanship trainer. The tactical training weapon fire simulator requires a kill zone that encompasses the entire target while the marksmanship trainer requires a kill zone which is only a small portion of the target. Hence, if a matrix of independent detectors is used on the target, as suggested by Reference [2], this means that only one detector would be illuminated by any one laser shot. This is contrasted with the MILES tactical system which may have several detectors illuminated at one shot and their individual signal outputs summed before the threshold is encountered. The summed outputs of the multiple MILES detector reduces the variances of the turbulence-induced laser signal. This would not be the case for the gunnery marksmanship target. Since each detector would be independent and have an independent threshold, the variance of the detected signal will be the same as that of the laser light itself propagating through the atmospheric turbulence. This variance will be higher than that in the MILES system.

Also, as pointed out in Section II and in Reference [2], the unbiased detectors of the MILES system are not adequate for the marksmanship training due to their loss of sensitivity in the presence of background sun illumination. To obviate this problem, reversed biased photo-diodes were suggested. These small photo-diodes are very much smaller than the MILES one square centimeter solar cell detectors. As a

consequence, the averaging effects realized by the large MILES detectors which reduced the fading effects of the turbulence would not occur in the smaller photo-diodes. This averaging phenomenon had an additional mitigating effect on the variance of the turbulence-induced fluctuation of the laser signal. It is because of lack of these averaging effects in the required detector for marksmanship that the electrical signal after detection will be identical to the statistics of the turbulence-induced laser light fluctuations.

In a previous report [1] a universal mathematical model was constructed for laser propagation through turbulence which could be used for the statistical analysis of laser weapon fire simulators. That model was based upon data gathered during March 1980 through experiments conducted at Kennedy Space Center's Shuttle Landing Facility. Although the universal model developed in the earlier report did permit evaluation of the theoretical statistical moments of the laser beam intensity fluctuations, its functional form did not lend itself to calculations involving the probability of detection which is the cumulative fade-time. So as to calculate the cumulative fade time at least at the long ranges, the so-called K-distribution was used. The data from the March 1980 experiments did show that the K-distribution was a reasonable approximation to the laser light scattering at the long ranges. It was the purpose of the present study to refine the earlier proposed universal math model so that the probabilities of detection for various thresholds could be calculated. Additional data was obtained during the last days in August 1980 at the Space Shuttle Landing Facility.

EXPERIMENTAL MEASUREMENTS

The propagation experiments conducted during August 1980 were the same as the earlier experiments in March 1980 and they are described in Reference [1]. These new measurements indicate that the data at a particular range from the transmitter can vary significantly depending upon the strength of the turbulence, C_n^2. The C_n^2 depends upon the air temperature, time of day, and even time of year. As in the previous data, we found that the mean-square fluctuations of the laser intensity normalized with respect to the square of the mean value of the laser signal reached a maximum value of approximately 6. From this high value, the normalized mean-square fluctuations decreased to the limiting value of 2.

Due to the strength of the turbulence during the August measurements, we found that the normalized moments of the laser intensity fluctuations at ranges of 2,500 - 3,000 meters were close to those of the negative exponential distribution. The negative exponential has long been recognized theoretically as the limiting distribution for the intensity fluctuations at very long distances under conditions of very strong turbulence. We believe this is the first time ever any research team has obtained data which comes so close to supporting this particular mathematical theory.

RESULTS

As in the previous report, the first five normalized moments $\langle I^n \rangle / \langle I \rangle^n$, n = 1,2,3,4,5 associated with the measured intensity fluctuations of the optical beam were calculated. In Figure 3-1 we have plotted the third, fourth, and fifth normalized moments as a function of the second

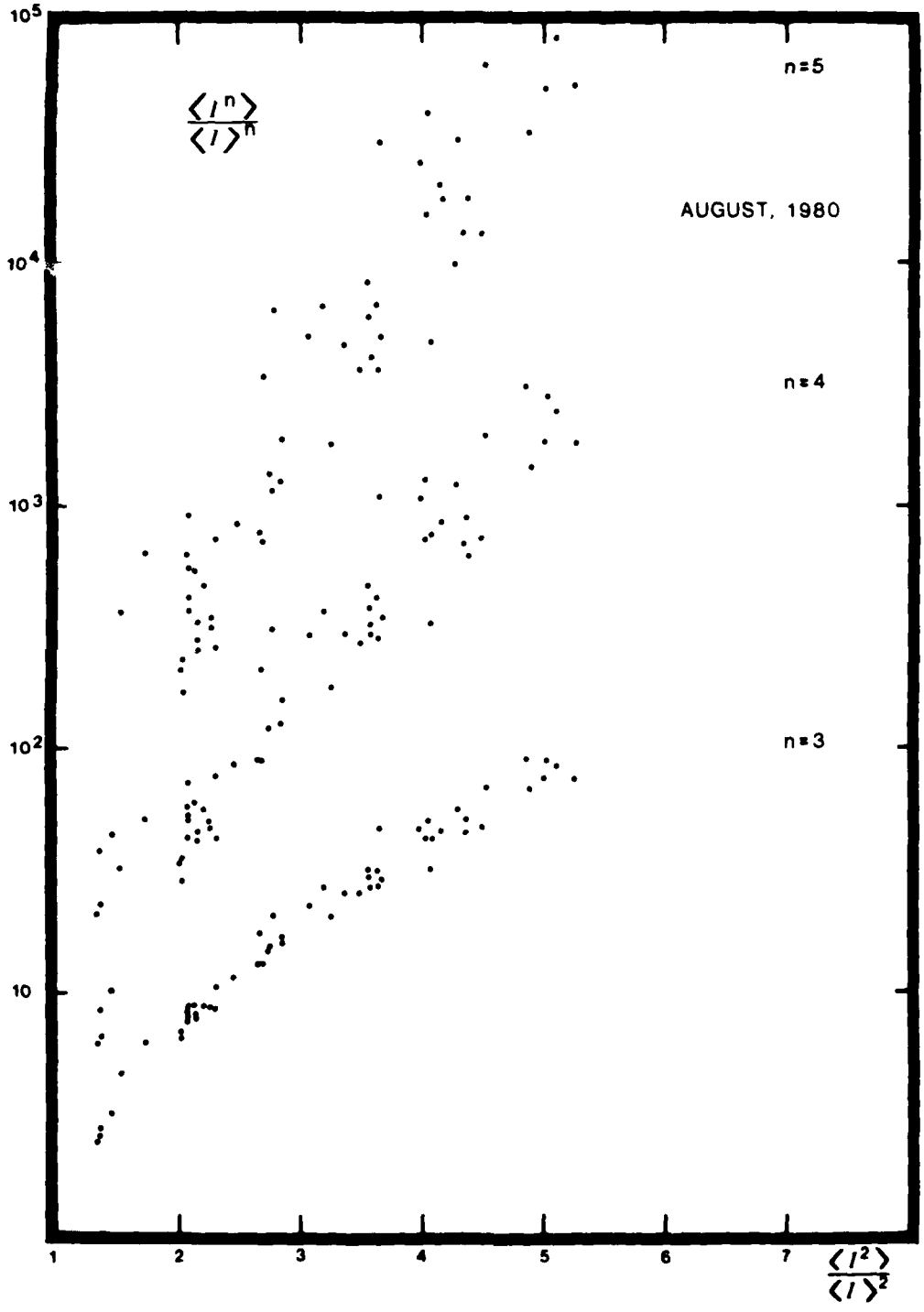

Fig. 3-1. Measured values of the normalized third, fourth and fifth moments obtained during August, 1980 experiments.

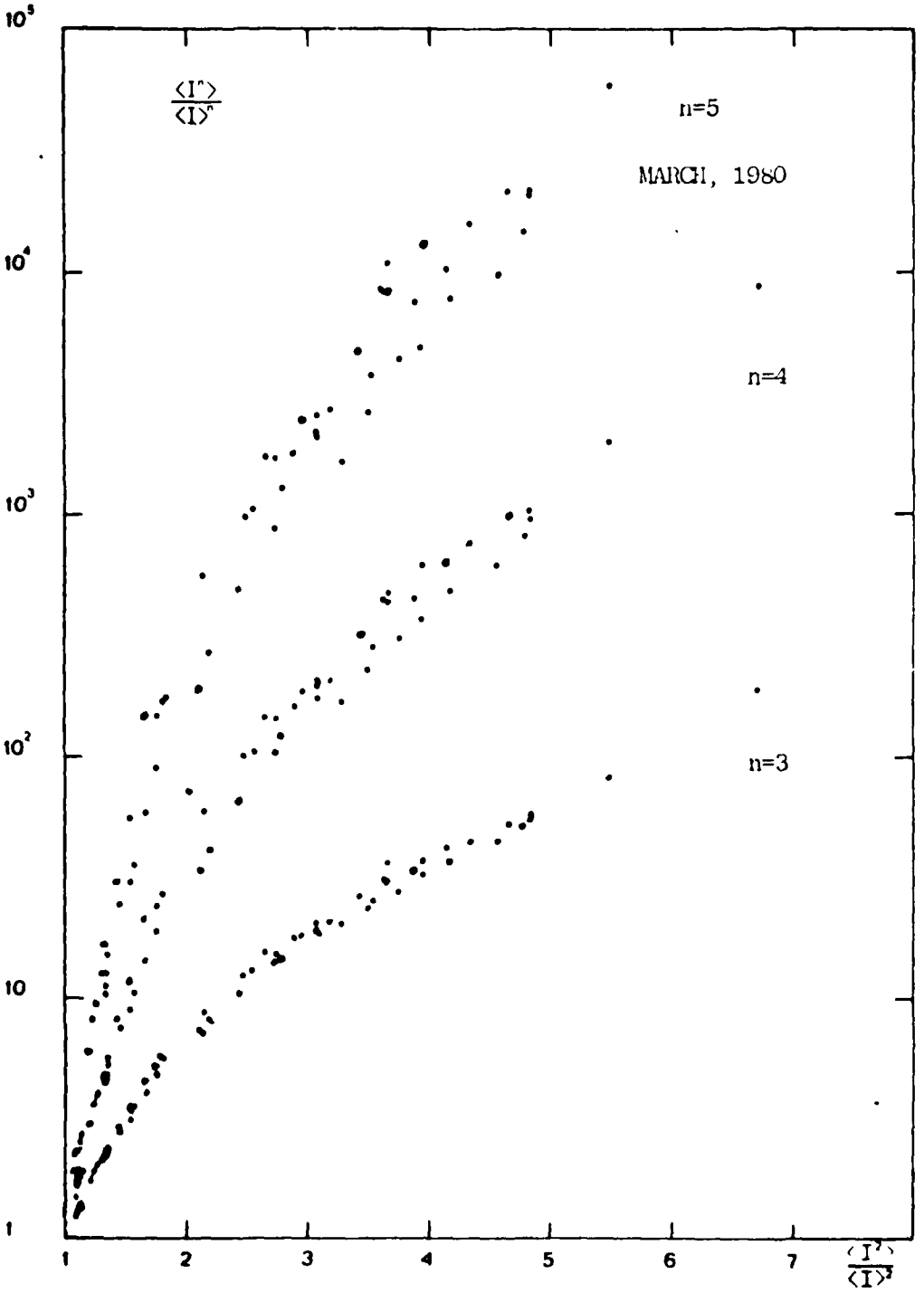

Fig. 3-2. Measured values of the normalized third, fourth and fifth moments obtained during March, 1980 experiments.

normalized moment $\langle I^2\rangle/\langle I\rangle^2$. The same data as taken in March is shown in Figure 3-2. In Figure 3-1 the data appears to be widely dispersed as compared with Figure 3-2. This is partly due to the fact that there was a lot more fluctuation in the C_n^2 from minute to minute during the August measurements as compared with the March measurements.

To better understand how the data changes as a function of distance and strength of turbulence, C_n^2, we have plotted the third normalized moment only as a function of the second normalized moment in Figures 3-3, and 3-4, illustrating the data at various distances and time of the day. The temperature is also a big factor in this data. To see how the data moves as a function of distance and/or structure constant C_n^2 , we have drawn a curve that we believe the data follows. That is to say, if data at various distances could all be obtained simultaneously for a particular value of the structure constant C_n^2, we believe the data would move along the lower curve shown as a function of distance until the normalized second moment, $\langle I^2\rangle/\langle I\rangle^2$, reached a value near 6 and then as the distance increased even more the data would be dispersed along the upper curve approaching the limiting point where $\langle I^2\rangle/\langle I\rangle^2 = 2$. Since the actual data obtained was gathered at different times of the day, the value of the structure constant C_n^2 changed by as much as two orders of magnitude during this time frame. This accounts for the fact that the data taken in August at 500 meters, which was taken from 2:15 p.m. to 2:51 p.m., appears to be closer to the limiting value $\langle I^2\rangle/\langle I\rangle^2 = 2$ than does the data at 1,000 meters which was taken from 4:29 p.m. to 4:56 p.m. Similarly, the data at 2,500 meters was taken from 2:32 p.m. to 3:08 p.m. while the data at 3,000 meters was

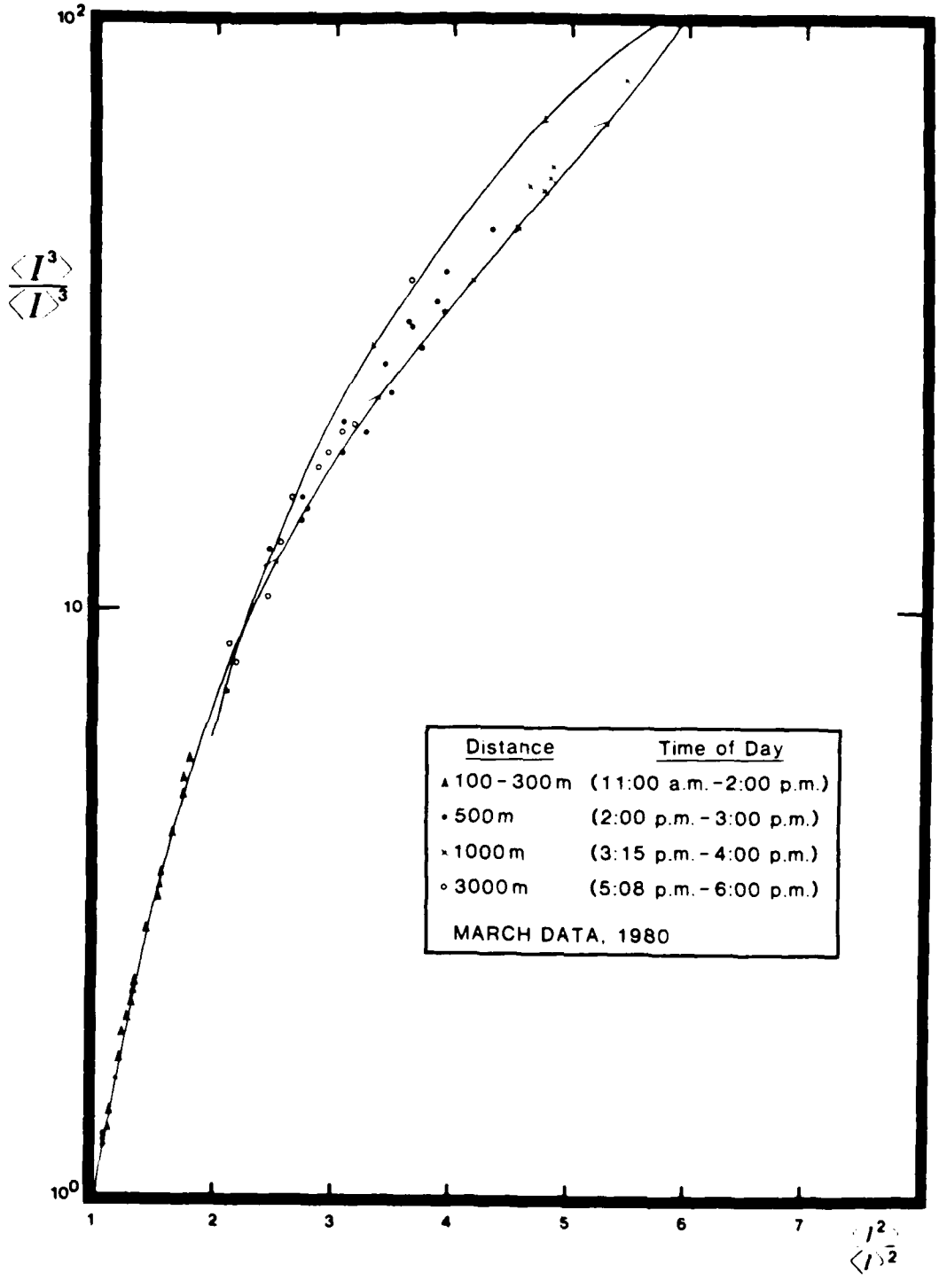

Fig. 3-3. Measured values of the normalized third moment obtained during March, 1980 experiments. The curve indicates movement of the data as a function of distance and/or structure constant.

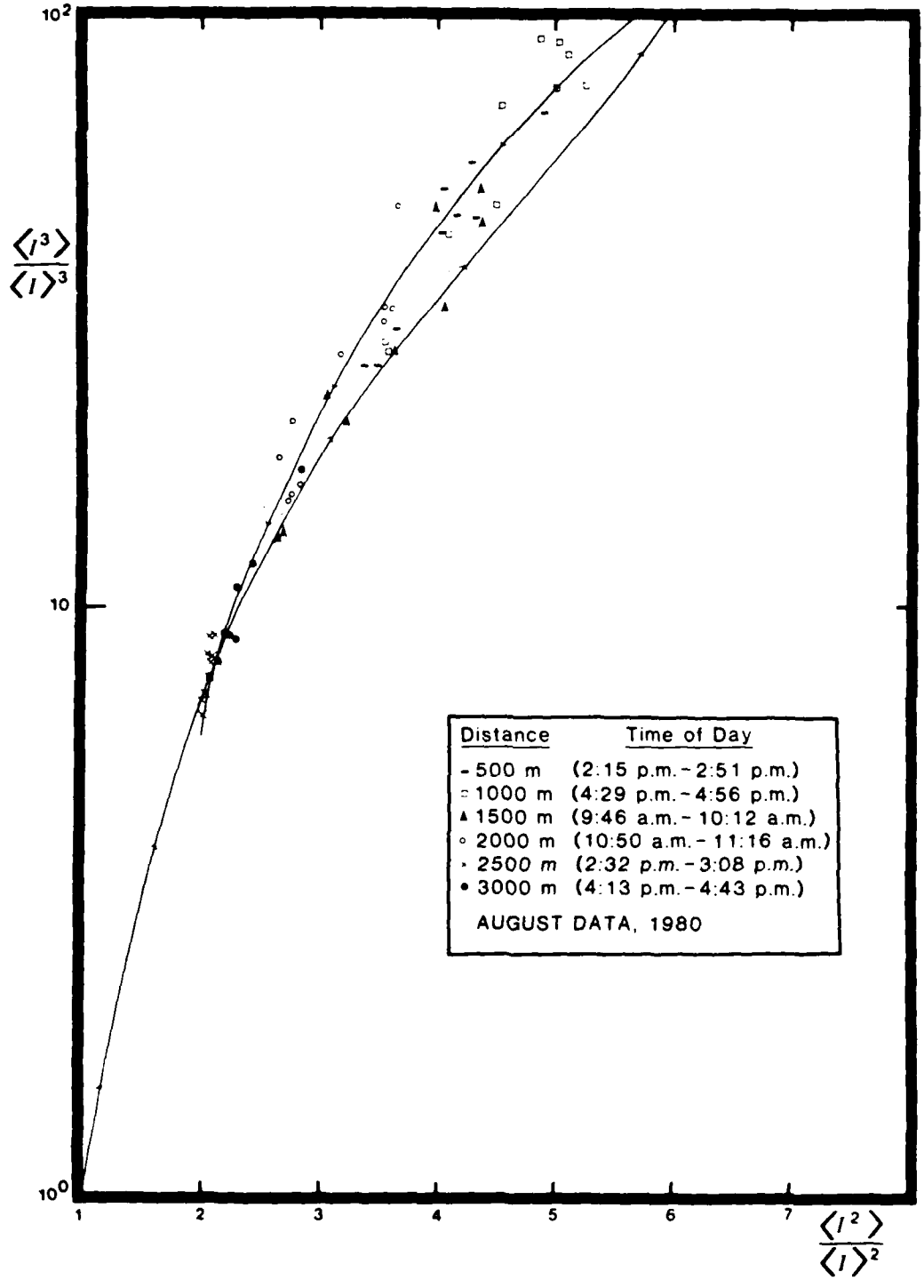

Fig. 3-4. Measured values of the normalized third moment obtained during August, 1980 experiments. The curve indicates movement of the data as a function of distance and/or structure constant.

taken from 4:13 p.m. to 4:43 p.m. Thus we were actually closer to the limiting value $\langle I^2\rangle/\langle I\rangle^2 = 2$ at 2,500 meters than we were at 3,000 meters. The time of day and temperature are very important factors, therefore, in determining the strength of the turbulence as well as the distance. During the August measurements, the value of the structure constant C_n^2 varied from 10^{-13} $m^{-2/3}$ to 10^{-11} $m^{-2/3}$. The values correspond to conditions of very strong turbulence.

UNIVERSAL MATH MODEL

Relying on arguments similar to those given in Section V of Reference [1], we assume the received field is composed of two principal components — the specular component resulting from the forward scattering by the large eddies along the propagation axis and the diffuse component caused by multiple scattering by the off-axis eddies. Thus the received field is mathematically represented by

$$U(t) = (Ae^{i\Theta} + Re^{i\phi})\, e^{i\omega t}, \tag{3.1}$$

where the first term corresponds to the specular component and the second term the diffuse component.

Over short propagation paths the field U(t) consists primarily of the specular component. Many arguments have been presented to suggest that the amplitude A of this specular component satisfies Log-Normal statistics. There is an abundance of data to support this assumption, including our own short-range data obtained during March and August experiments [1]. However, over longer propagation paths it is not clear what statistics the amplitude A will satisfy since the amplitude

of the field will consist of both specular and diffuse components rather than the specular component alone. In our previous model we made the assumption that A remained Log-Normal for all propagation path lengths. From a modeling standpoint this assumption limits some of the flexibility of the model to fit the experimental data. We now believe that it is more meaningful to assume that A is associated with a more general distribution than the Log-Normal distribution, but one which exhibits the characteristics of the Log-Normal distribution at least over short propagation path lengths. That is to say, the distribution should contain certain parameters that can be selected from comparisons with experimental data and which have the effect of changing the characteristics of the probability distribution as the parameters change. A general distribution of this type is the m-distribution defined by

$$p(A) = \frac{2M^M A^{2M-1}}{\Gamma(M)\, c^M} e^{-MA^2/c}, \quad A > 0 \tag{3.2}$$

where $c = \langle A^2 \rangle$ is the average of the intensity A^2 and M is the primary parameter that controls the characteristics of the distribution. The function $\Gamma(.)$ is the gamma function ([3], pp. 253-294).

For large values of M, the m-distribution behaves like a Log-Normal distribution (see Appendix A), for $M = \frac{1}{2}$ it is Gaussian in functional form, while for M = 1 it becomes the well-known Rayleigh distribution. Hence the m-distribution seems appropriate here because of the close relationship it bears to the standard distributions associated with communication theory.

The amplitude R of the diffuse component is also assumed to be m-distributed, i.e.,

$$p(R) = \frac{2m^m R^{2m-1}}{\Gamma(m)\, b^m} \; e^{-mR^2/b} \tag{3.3}$$

This is the same assumption we previously made in Reference [1] and the reasons for it are likewise stated there. Also as before, we assume that both phase angles Θ and ϕ are uniformly distributed, and finally that all random variables are independent.

A. Development of the PDF:

Our previous development of the PDF given in Reference [1] lead to an expression that was difficult to use for numerical calcalations of the cumulative distribution function. The present development, although similar in nature, leads to a simpler functional form from which calculations can be more easily obtained. The intensity of the field (3.1) is

$$I = |U(t)|^2 = A^2 + R^2 + 2AR \cos(\phi - \Theta). \tag{3.4}$$

Following the technique outlined in [1], the PDF is determined from the relation

$$p(I) = \tfrac{1}{2} \int_0^\infty z\, C(z)\, J_0(\sqrt{I}\, z)\, dz \tag{3.5}$$

where

$$C(z) = \int_0^\infty p(A)\, J_0(Az)\, dA \int_0^\infty p(R)\, J_0(Rz)\, dR. \tag{3.6}$$

The function $J_0(.)$ is the standard Bessel function of zero order ([3], pp. 355-434). The evaluation of these integrals, which is given in

Appendix B, leads to the infinite series representation

$$p(I) = \frac{m\Gamma(m)}{b\Gamma(M)} e^{-mI/b} \sum_{k=0}^{\infty} \frac{(-1)^k}{k!} L_k\left(\frac{mI}{b}\right) \sum_{j=0}^{\infty} \binom{k}{j}^2 \frac{\Gamma(M + j)\,(rm/M)^j}{\Gamma(m - k + j)} \tag{3.7}$$

where

$$\binom{k}{j} = \frac{k!}{j!(k - j)!} \tag{3.8}$$

is the binomial coefficient and L_k denotes the Laguerre polynomials [3].

The paramter r appearing in (3.7) is the power ratio of the specular to diffuse components, i.e.,

$$r = c/b. \tag{3.9}$$

Over short propagation path lengths the parameter r is very large and monotomically decreases to zero as the strength of the turbulence increases and the path length increases. In fact, the limiting form of (3.7) is obtained by letting $r \to 0$ and $m \to 1$, which leads to

$$p(I) = \frac{1}{b} e^{-I/b}. \tag{3.10}$$

This limiting form is the negative exponential distribution which has been strongly supported by reasearchers over the years.

B. Theoretical Moments:

The statistical moments of the intensity I are computed from the expression

$$\langle I^n \rangle = \int_0^{\infty} I^n\, p(I)\, dI, \quad n = 1,2,\ldots \tag{3.11}$$

from which we get (see Appendix C)

$$\langle I^n \rangle = \left(\frac{b}{m}\right)^n \sum_{k=0}^{n} \binom{n}{k}^2 \frac{\Gamma(M + k)\, \Gamma(m + n - k)}{\Gamma(M)\, \Gamma(m)} \left(\frac{rm}{M}\right)^k \quad (3.12)$$

For purposes of comparing the theoretical moments with those obtained from experimental data it is necessary to normalize them. This we do by first setting n=1 to find the mean

$$\langle I \rangle = b(1 + r), \quad (3.13)$$

and then dividing (3.12) by $\langle I \rangle^n$. This action results in the expression

$$\frac{\langle I^n \rangle}{\langle I \rangle^n} = \frac{1}{(1 + r)^n} \sum_{k=0}^{n} \binom{n}{k}^2 \mu_{n-k}\, a_k\, r^k, \quad (3.14)$$

where we have introduced the notation

$$\mu_k = \frac{\langle R^{2k} \rangle}{\langle R^2 \rangle^k} = \frac{\Gamma(m + k)}{m^k\, \Gamma(m)} \quad (3.15)$$

and

$$a_k = \frac{\langle A^{2k} \rangle}{\langle A^2 \rangle^k} = \frac{\Gamma(M + k)}{M^k\, \Gamma(M)} \quad (3.16)$$

Eq. (3.14) has the same functional form as Eq. (5.19) in Reference [1]. The primary distinction is that the normalized moments a_k of the specular component and now associated with the m-distribution rather than the Log-Normal distribution.

In order to match the theoretical moments (3.14) with actual data obtained from field experiments, we have to appropriately select three parameters: m, M and r. We do this in such a way that the first two normalized moments of I match the data identically and the third moment

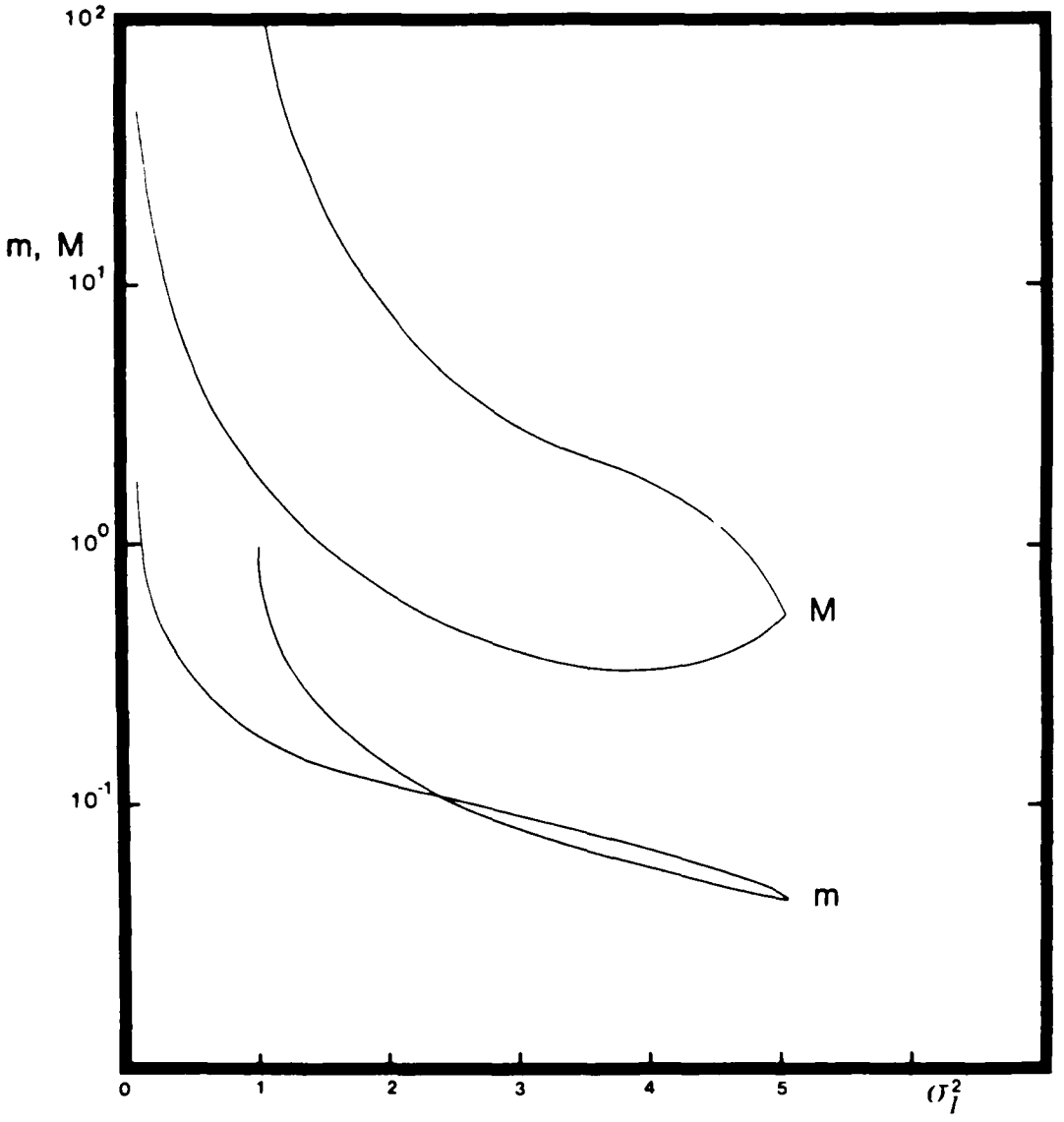

Fig. 3-5. Parameters of the m-distributions associated with the diffuse and specular components of the laser beam as a function of the normalized variance.

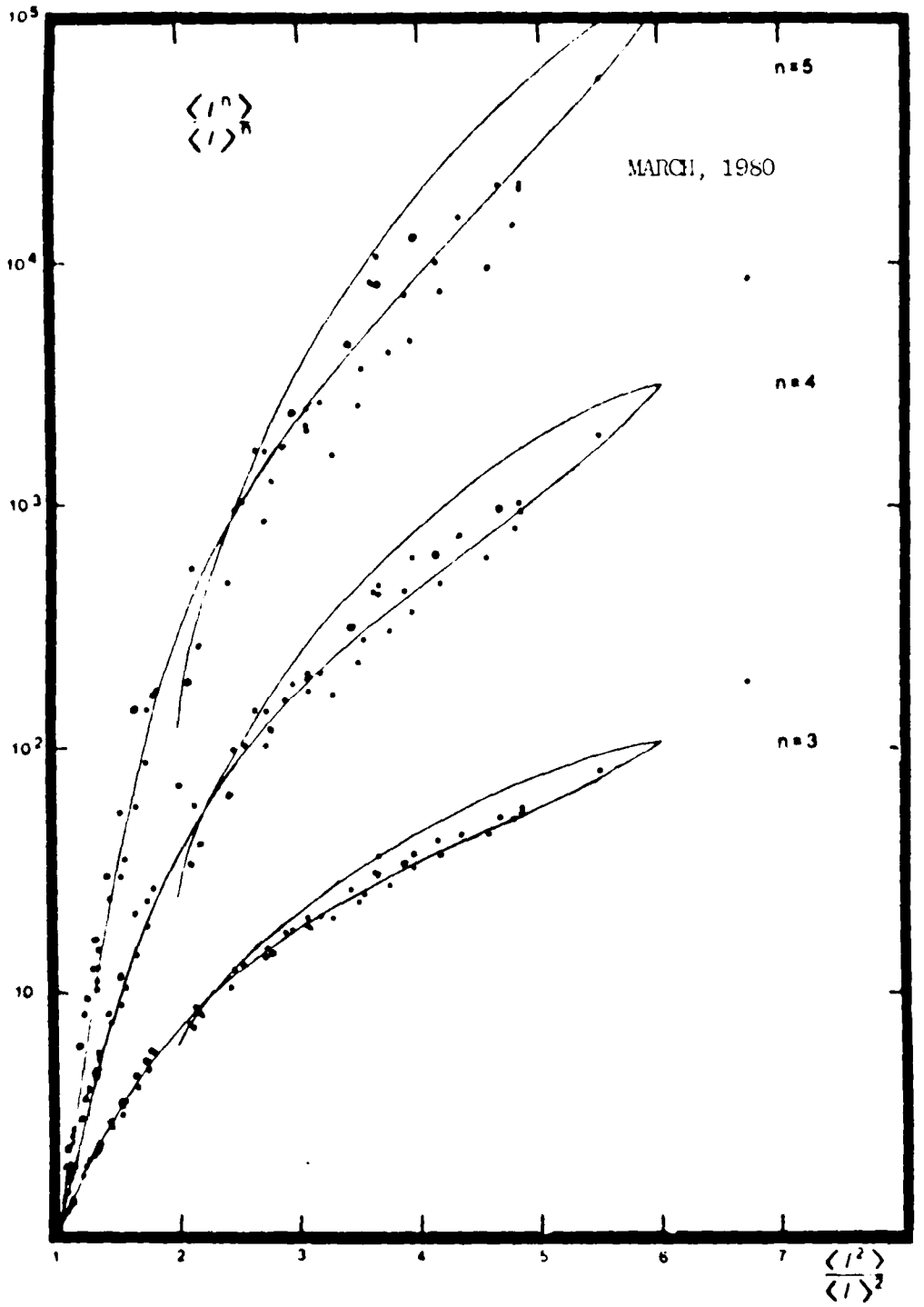

Fig. 3-6. Measured values of the normalized third, fourth and fifth moments obtained during March, 1980 experiments and compared with values expected from the universal model.

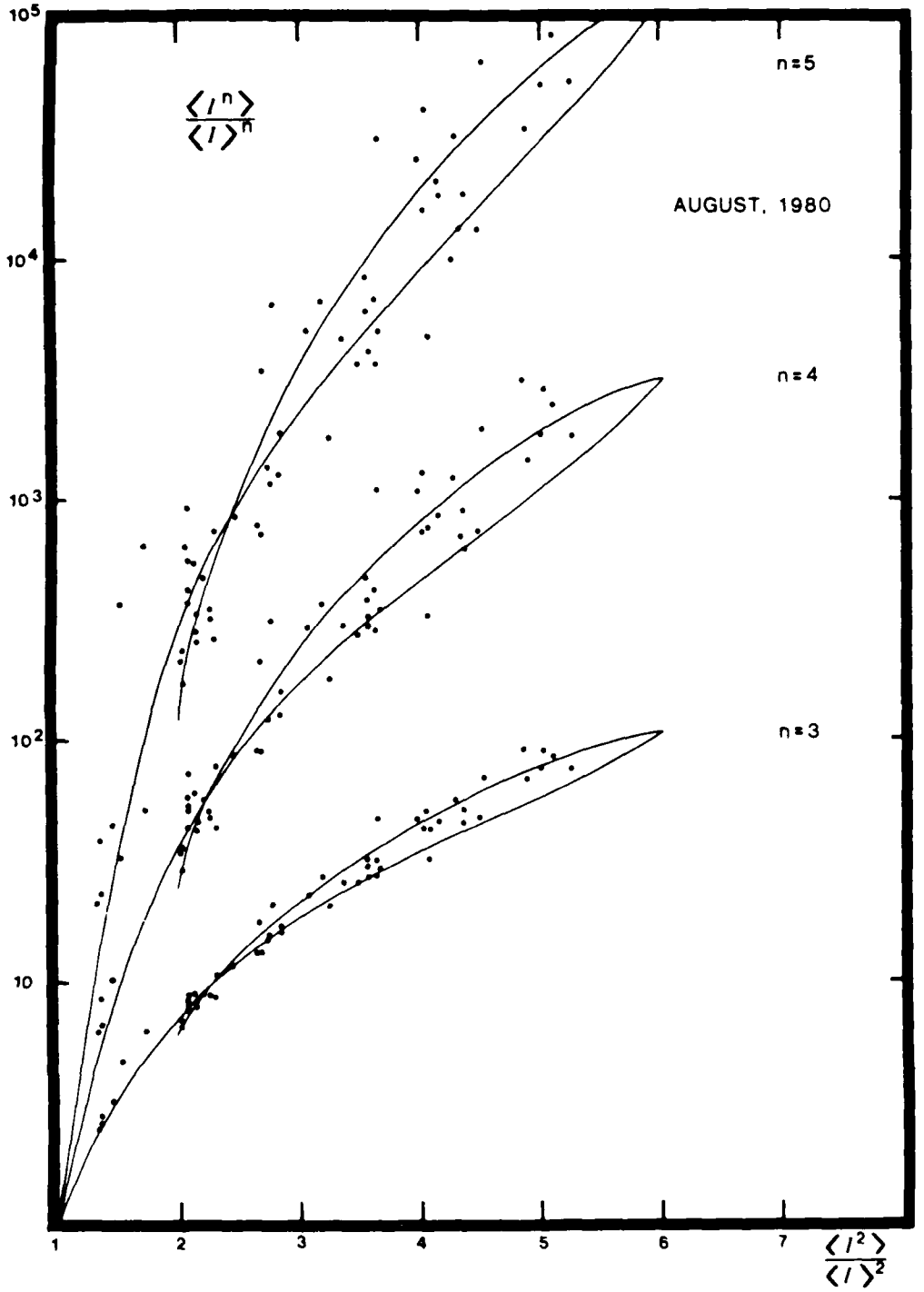

Fig. 3-7. Measured values of the normalized third, fourth and fifth moments obtained during August, 1980 experiments and compared with values expected from the universal model.

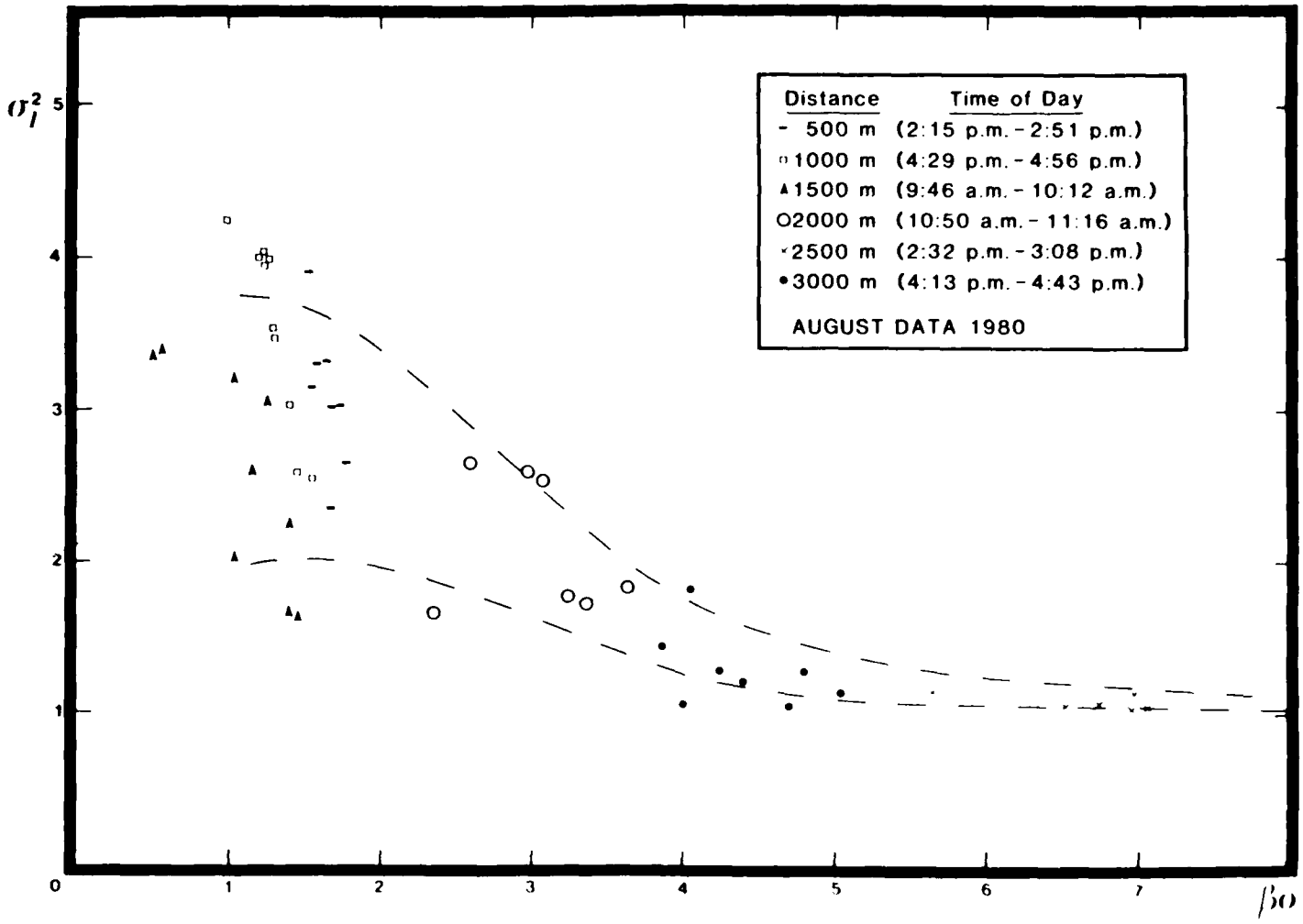

Fig. 3-8. Measured normalized variance versus f_0. The dashed curves represent possible upper and lower bounds for theoretical curves.

is then matched by some "best fit" criterion.

The parameters m and M as a function of the normalized variance σ_I^2 that appeared to give the best visual fit to the data are graphed in Figure 3-5. The remaining parameter r is then calculated from the formula

$$r = \frac{2 - \chi + \sqrt{(a_2 + \mu_2 - 4)\chi + 4 - a_2\mu_2}}{\chi - a_2} , \qquad (3.17)$$

where $a_2 = 1 + 1/M$, $\mu_2 = 1 + 1/m$ and $\chi = \langle I^2 \rangle / \langle I \rangle^2$. Eq. (3.17) is equivalent to Eq. (5.24) in [1]. The resulting theoretical curves along with the data obtained in March and August, respectively, are shown in Figures 3-6 and 3-7.

The three parameters m, M and r of our theoretical model have been tied to the normalized variance σ_I^2 as suggested above. The variance as a function of the parameter $\beta_o = (0.5\ C_n^2\ k^{7/6}\ L^{11/6})^{\frac{1}{2}}$, where C_n^2 is the structure constant, k is the wave number of the optical beam, and L is the path length, is shown in Figure 3-8 for the actual data obtained in August. The data is widely scattered, as discovered also by other researchers, so that a single curve drawn through the data does not seem feasible at this time. The dashed curves that we have drawn suggest possible upper and lower bounds for the normalized variance as a function of β_o.

C. Cumulative Distribution:

To derive the cumulative distribution function from which the fading probabilities (and hence, the detection probabilities) can be computed, we first normalize the density function (3.7) so that the

mean value is unity. Thus by introducing the normalized variable $y = I/\langle I \rangle$, we see that (3.7) becomes

$$p(y) = \frac{(1 + r)\, m\Gamma(m)}{\Gamma(M)}\, e^{-(1 + r)\, my} \sum_{k=0}^{\infty} \frac{(-1)^k}{k!} L_k[(1 + r)\, my]$$

$$\times \sum_{j=0}^{k} \binom{k}{j}^2 \frac{\Gamma(M + j)}{\Gamma(m + j - k)} (rm/M)^j \qquad (3.18)$$

The probability of detection P_d is then defined by

$$P_d = \int_T^{\infty} p(y)\, dy \qquad (3.19)$$

for a specified threshold value $T = I_T/I_o$, where I_o is the mean value of intensity. Through application of the integral formula ([4], p. 844)

$$\int_y^{\infty} e^{-x} L_n(x)\, dx = e^{-y} [L_n(y) - L_{n-1}(y)] \qquad (3.20)$$

we immediately find that

$$P_d = e^{-z} \left\{ 1 + \frac{\Gamma(m)}{\Gamma(M)} \sum_{k=1}^{\infty} \frac{(-1)^k}{k!} [L_k(z) - L_{k-1}(z)] \right.$$

$$\left. \times \sum_{j=0}^{k} \binom{k}{j}^2 \frac{\Gamma(M + j)}{\Gamma(m + j - k)} (rm/M)^j \right\} \qquad (3.21)$$

where

$$z = (1 + r)\, mT. \qquad (3.22)$$

The probability of fade P_d is therefore

$$P_f = 1 - P_d \qquad (3.23)$$

The fade and detection probabilities associated with long-range propagation paths for which $\sigma_I^2 = 1.5$ are shown in Figure 3-9 for the universal math model described here as well as similar curves predicted by the Log-Normal and K-distribution models. For low threshold values we find the Log-Normal model predicting a much higher probability of detection than our universal model, while the K-distribution gives cumulative probabilities that closely resemble the universal math model as we previously suggested in Reference [1]. As the variance decreases for longer ranges to the limit value $\sigma_I^2 = 1$, we have found that the K-distribution curves approach those predicted by the negative exponential model in a manner similar to our universal model. In Figure 3-10 we have shown how this limiting cumulative distribution curve (depicted by the dashed curve) is approached for decreasing variance (corresponding to increased path lengths) from a value of $\sigma_I^2 = 3.5$ to $\sigma_I^2 = 1$.

For variances such that $\sigma_I^2 > 1.5$ at long distances the K-distribution deviates more strongly from the cumulative distribution curves predicted by the universal math model. For that reason we do not believe the K-distribution represents a good model for these values of the variance which correspond to more intermediate path lengths and conditions of turbulence.

For short ranges and thresholds such that $T \geqq 0.4$ we find little distinction between the cumulative probability curves as predicted by the Log-Normal model and the universal model. However, for lower threshold values the log-normal model predicts a higher probability of detection than does the universal model. Some representative curves of the universal model for the cumulative probabilities are shown in Figure 3-11 corresponding to variances of $\sigma_I^2 = 0.5, 1.0, 2.5$.

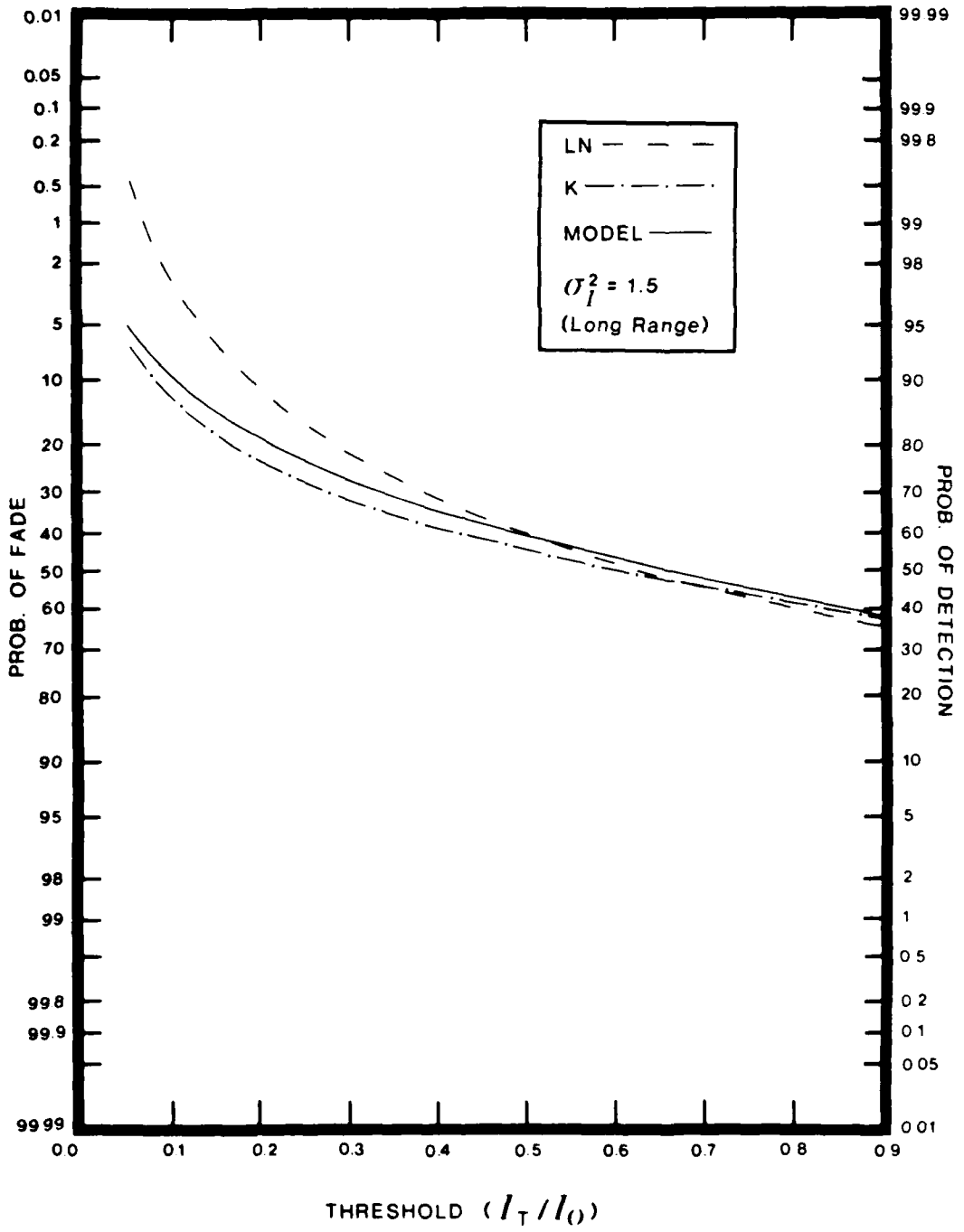

Fig. 3-9. Comparison of cumulative fading models at long ranges for the K-distribution, the Log-Normal distribution and the universal model as a function of the ratio of receiver threshold to mean intensity.

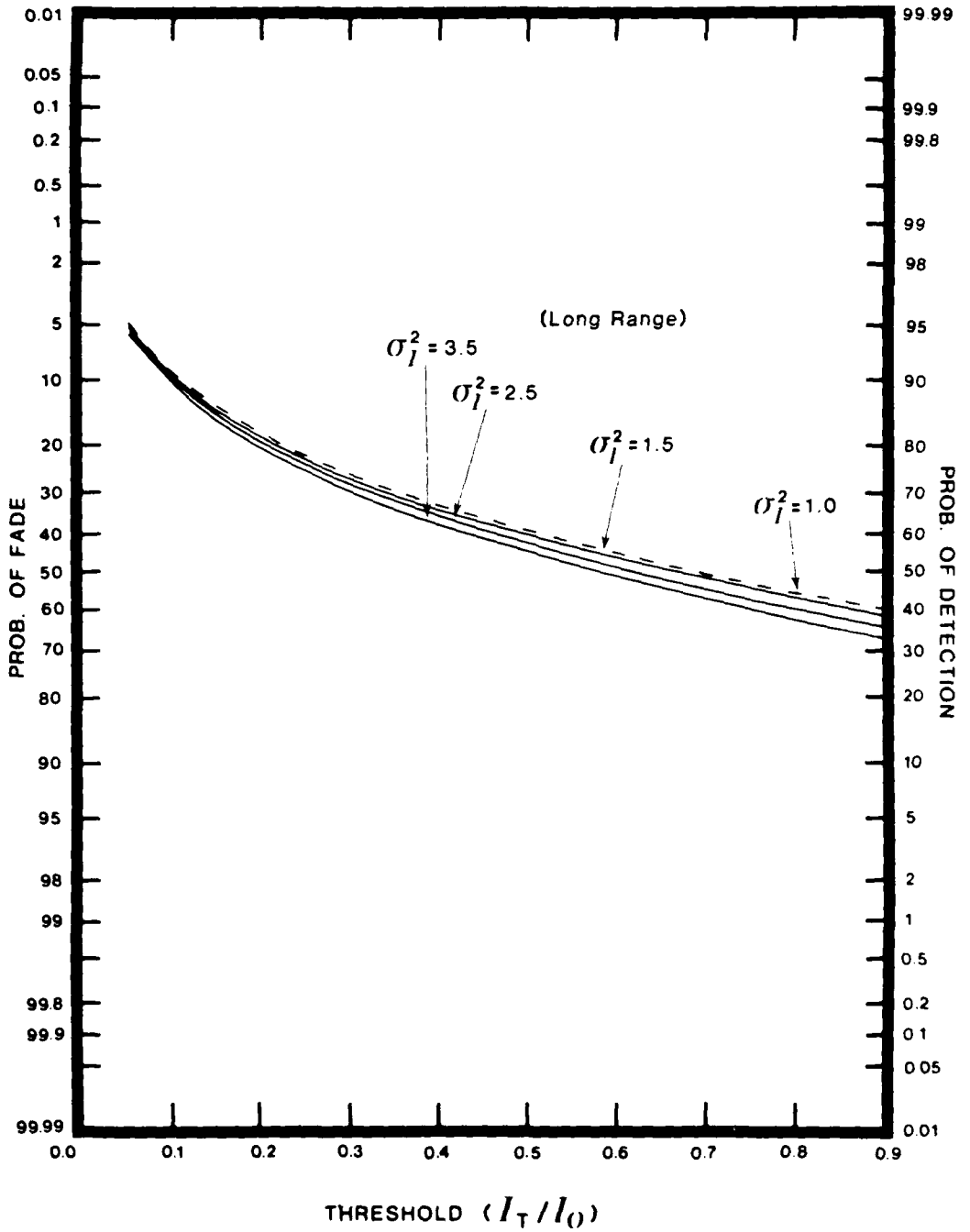

Fig. 3-10. Probability of fade curves as predicted by the universal model for long ranges with different variances. The dashed curve is the limiting curve predicted by the negative exponential model for extremely long ranges or conditions of turbulence.

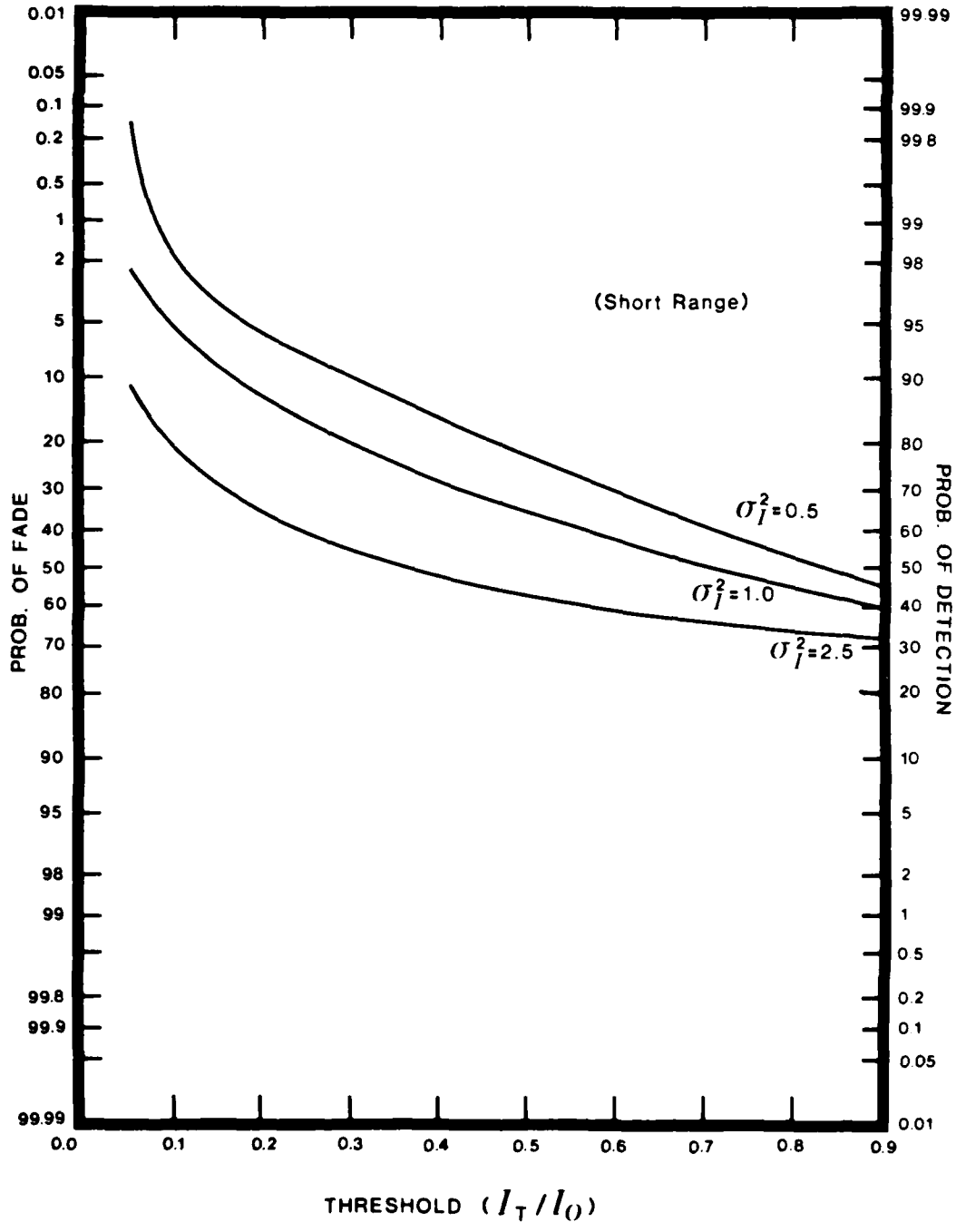

Fig. 3-11. Probability of fade curves as predicted by the universal model for short ranges with different variances.

SECTION IV

CONCLUSIONS

The MILES system was designed as a tactical weapon fire simulator. The kill zone was tailored to have a shape so as to have an approximate kill probability equal to the kill probability of a particular weapon engaging a particular target. To do this the beam was made wide enough to illuminate several detectors for any well-aimed shot. In some instances, the entire target would be illuminated by the laser beam. The output of each of the illuminated detectors was summed and then discriminated against a fixed threshold. There was no attempt to simulate the hit of a round on any particular location on the target. The tested MILES system as currently configured would make a very poor gunnery marksmanship trainer. The following list of recommendations are proposed as MILES add-on which would allow the MILES system to be used as a marksmanship trainer.

RECOMMENDATIONS

1. Replace MILES solar cell detectors with reversed biased photodiodes.
2. Replace MILES detector belts with a matrix of independent detectors each with its own pre-amplifier and discriminator threshold. The MILES pre-amplifier and discriminator can be retained.
3. Retain the MILES decoder box, but one must be used for each detector.

4. Replace MILES laser transmitter with transmitter with much smaller beam divergence and more beam uniformity. This will ensure a single narrow gaussian beam as opposed to the wide MILES tri-gaussian beam.
5. Retain the MILES encoder which is used to drive the transmitter with standard MILES codes.

If these recommendations are implemented, the following questions would require answers:

a. What should be the transmitter power?
b. What should be the transmitter beam divergence?
c. What should be the photo-diode detector spacing on the target?

To begin to answer these system design questions, the receiver structure must be defined and the atmospheric optical communication channel statistics must be modelled. The NTEC research team proposed a CW laser transmitter operating at a high PRF and a phase-locked loop or a matched filter receiver. The NTEC receivers and CW laser high PRF transmitter also requires a knowledge of the optical communication channel statistics so that the pulse rate of the transmitter can be set and the optimum threshold of the receiver can be established.

The statistical model developed by the UCF research team established the statistical moments and the cummulative fading as a function of the threshold setting of the discriminator. The following observations can be made about the statistical model of the optical communication channel:

1. The measured long range statistics were Negative Exponential as shown in Equation 3-10. This is the first time this statistic has ever been measured although it has been theoretically predicted for some ten years.
2. The developed math model matches the Log-Normal statistic at short ranges and the asymptotic long-range Negative Exponential statistic.
3. The intermediate ranges have the lowest probability of detection or rather the greatest cummulative fading.
4. The detection probability gets better at the very long ranges.
5. The amount of scattering can vary considerably at a fixed range. For example at 2,000 meters the detection probability may be at one value and then when the scattering gets stronger the detection probability may actually improve. Conversely, if the scattering would weaken, it is possible the detection probability may actually get worse.
6. The threshold setting of the receiver should be determined using tne worst case using intermediate range statistics.

The system parameters can be set using the math model developed here, but to set the PRF of the proposed NTEC CW laser transmitter, the average length of fade time needs to be determined. This math model was not part of this project, but if the development of the proposed NTEC system continues, that math model must be constructed. The m-distribution used in the analysis would form the basis for the math model of the average fade period as a function of the receiver threshold.

The combined UCF and NTEC study suggests that the CW laser high PRF transmitter and receiver be developed as MILES add-ons for long-range gunnery marksmanship training. To set the parameters of that CW laser system, a math model for the average fade period would be required.

REFERENCES

[1] R. L. Phillips and L. C. Andrews, "Laser Marksmanship Potential Evaluation: Math Modeling and Experimental Verification," Final Report prepared for U.S. Army Project Manager for Training Devices, Contract No. N61339-79-D-0105 (July 1980)

[2] A. Marshall, B. Shaw, and G. Bond, "Laser Marksmanship Potential Evaluation," Final Report prepared for U.S. Army Project Manager for Training Devices, PM TRADE-RE-0007, (November 1980)

[3] M. Abramowitz and I. A. Stegun , eds., Handbook of Mathematical Functions, Dover (1965)

[4] I.S. Gradshteyn and I. W. Ryzhik, Table of Integrals, Series and Products, *Academic Press, New York (1980)*

[5] A. Erdelyi, et al, Higher Transcendental Functions, Vols. 1 and 2, Bateman Manuscript Project, McGraw-Hill (1953)

[6] L. A. Mallette, "Modeling the Silicon Solar Cell as an Optical Detector," Master's Thesis, University of Central Florida, Orlando (1977)

APPENDIX A

LOG-NORMAL APPROXIMATION TO THE m-DISTRIBUTION

The m-distribution

$$p(A) = \frac{2M^M}{\Gamma(M)c^M} A^{2M-1} e^{-MA^2/c}, \tag{A-1}$$

for large values of the parameter M, can be closely approximated by the Log-Normal distribution. To see how this comes about, we start by introducing the change of variables

$$\frac{A^2}{c} = e^x \tag{A-2}$$

so that (A-1) becomes

$$p(x) = \frac{M^M}{\Gamma(M)} e^{Mx} \exp(-Me^x). \tag{A-3}$$

Under the assumption that $x << 1$ (i.e., $A^2 << c$), we can use the approximation

$$e^x \cong 1 + x + \tfrac{1}{2} x^2$$

in (A-3) from which we get

$$p(x) \cong \frac{M^M}{\Gamma(M)} e^{Mx} \exp[-M(1 + x + \tfrac{1}{2}x^2)]$$

$$\cong \frac{M^M}{\Gamma(M)} e^{-M} \exp(-Mx^2/2). \tag{A-4}$$

Now returning to the original variable by use of (A-2), we see that

$$p(A) \cong \frac{2M^M e^{-M}}{\Gamma(M)\, A} \exp\left[\frac{-M}{2}\left(\log A^2 - \log c\right)^2\right]. \qquad \text{(A-5)}$$

Finally, we invoke Stirling's formula ([3], p. 257)

$$\Gamma(M) \sim e^{-M} M^{M-\frac{1}{2}} \sqrt{2\pi}\,, \quad M >> 1$$

from which we deduce

$$p(A) \cong \frac{(2M/\pi)^{\frac{1}{2}}}{A} \exp\left[-\frac{M}{2}\left(\log A^2 - \log c\right)^2\right]$$

or equivalently

$$p(A) \cong \frac{1}{\sqrt{2\pi}\, A\, \sigma_{LN}} \exp\left[\frac{-(\log A - \frac{1}{2}\log c)^2}{2\,\sigma_{LN}^2}\right] \qquad \text{(A-6)}$$

where we have set $M = 1/\sigma_{LN}^2$. Clearly, Eq. (A-6) is the Log-Normal distribution.

APPENDIX B

DERIVATION OF THE PDF

From Eq. (5.6) in Reference [1], we have

$$\int_0^\infty p(R)\, J_0(Rz)\, dR = {}_1F_1(m;\, 1;\, -bz^2/4m) \qquad \text{(B-1)}$$

where ${}_1F_1(a;\, b;\, c)$ is the confluent hypergeometric function ([3], pp. 503-536). Similarly we find

$$\int_0^\infty p(A)\, J_0(Az)\, dz = {}_1F_1(M;\, 1;\, -\, cz^2/4M) \qquad \text{(B-2)}$$

so that Eq. (3.6) in Section III leads to the result

$$C(z) = {}_1F_1(M;\, 1;\, -\, cz^2/4M)\ {}_1F_1(m;\, 1;\, -bz^2/4m) \qquad \text{(B-3)}$$

Next we employ Kummer's transformation ([3], p. 505)

$${}_1F_1(a;\, b;\, -x) = e^{-x}\ {}_1F_1(b - a;\, b;\, x)$$

so that

$$C(z) = e^{-bz^2/4m}\ {}_1F_1(M;\, 1;\, -\, cz^2/4M)\ {}_1F_1(1 - m;\, 1;\, bz^2/4m), \qquad \text{(B-4)}$$

and finally we use the formula ([5], p. 187)

$${}_1F_1(a;\, c;\, px)\ {}_1F_1(a';\, c';\, qx)$$

$$= \sum_{k=0}^{\infty} \frac{(a)_k\, (px)^k}{k!\ (c)_k}\ {}_3F_2(a',\, 1 - c - k,\, -\, k;\, c',\, 1 - a - k;\, -\, q/p)$$

where

$$(a)_k = \frac{\Gamma(a + k)}{\Gamma(a)}\ , \quad k = 0,1,2,\ldots$$

is the Pochhammer symbol and ${}_3F_2(a,b,c;\ d,e;\ x)$ is a generalized hypergeometric function, to obtain

$$C(z) = e^{-bz^2/4m} \sum_{k=0}^{\infty} \frac{(1 - m)_k \ (bz^2/4m)^k}{(k!)^2} \qquad \text{(B-5)}$$

$$\times \ {}_3F_2(M,\ -k,\ -k;\ 1,\ m - k;\ cm/bM).$$

The substitution of (B-5) into the integral

$$p(I) = \tfrac{1}{2} \int_0^{\infty} zC(z)\ J_0(\sqrt{I}z)\ dz \qquad \text{(B-6)}$$

and the subsequent interchange of integration with summation, together with the integral formula ([4], p. 718)

$$\int_0^{\infty} e^{-x^2}\ x^{2n+1}\ J_0(2x\ \sqrt{z})\ dx = \frac{n!}{2}\ e^{-z}\ L_n(z),$$

leads to the expression

$$p(I) = \frac{m}{b}\ e^{mI/b} \sum_{k=0}^{\infty} \frac{(1 - m)_k}{k!}\ L_k(mI/b) \qquad \text{(B-7)}$$

$$\times \ {}_3F_2(M,\ -k,\ -k;\ 1,\ m - k;\ cm/bM)$$

Replacing ${}_3F_2(;\ ;)$ with its series representation and simplifying, we finally get Eq. (3-7).

APPENDIX C

DERIVATION OF THE THEORETICAL MOMENTS

Starting with the equation

$$\langle I^n \rangle = \int_0^\infty I^n \, p(I) \, dI, \quad n = 1,2,\ldots, \tag{C-1}$$

where $p(I)$ is given by (3.7), and employing the integral formula ([4], p. 844)

$$\int_0^\infty e^{-st} \, t^\beta \, L_n(t) \, dt = \Gamma(\beta + 1) \, s^{-(\beta + 1)} \, F(-n, \beta + 1; 1; 1/s)$$

we find

$$\langle I^n \rangle = \left(\frac{b}{m}\right)^n \frac{\Gamma(m)}{\Gamma(M)} \sum_{k=0}^{\infty} \frac{(-1)^k}{k!} \, n! \, F(-k, n + 1; 1; 1)$$

$$\times \sum_{j=0}^{\infty} \binom{k}{j}^2 \frac{\Gamma(M + j)}{\Gamma(m + j - k)} \, (rm/M)^j, \tag{C-2}$$

where $F(a,b; c; x)$ is the hypergeometric function. Using the relation ([3], p. 556)

$$F(a,b; c; 1) = \frac{\Gamma(c) \, \Gamma(c - a - b)}{\Gamma(c - a) \, \Gamma(c - b)}$$

we find in our case

$$F(-k, n + 1; 1; 1) = \frac{\Gamma(k - n)}{\Gamma(k + 1) \, \Gamma(-n)}$$

$$= \begin{cases} (-1)^k \, n!/k!(n - k)! \, , & k \leq n \\ 0 \, , & k > n \end{cases} \tag{C-3}$$

and therefore (C-2) becomes

$$\langle I^n \rangle = \left(\frac{b}{m}\right)^n \sum_{k=0}^{n} \sum_{j=0}^{k} \frac{(n!)^2\, \Gamma(m)\, \Gamma(M + j)\, (rm/M)^j}{(n - k)!(j!)^2\, [(k - j)!]^2\, \Gamma(M)\, \Gamma(m + j - k)} \tag{C-4}$$

Eq. (C-4) has the functional form

$$\langle I^n \rangle = \left(\frac{b}{m}\right)^n \sum_{k=0}^{n} \sum_{j=0}^{k} C(k, j) \tag{C-5}$$

so that making the change of indices $p = k - j$ we have

$$\langle I^n \rangle = \left(\frac{b}{m}\right)^n \sum_{j=0}^{n} \sum_{p=0}^{n-j} C(p + j, j)$$

or

$$\langle I^n \rangle = \left(\frac{b}{m}\right)^n \sum_{j=0}^{n} \frac{(n!)^2\, \Gamma(M + j)\, (rm/M)^j}{\Gamma(M)\, (j!)^2\, (n - j)!} \times \sum_{p=0}^{n-j} \frac{(n - j)!\, \Gamma(m)}{(n - p - j)!\, \Gamma(m - p)(p!)^2}$$

However, the second series in (C-6) reduces to

$$\sum_{p=0}^{n-j} \frac{(n - j)!\, \Gamma(m)}{(n - p - j)!\, \Gamma(m - p)\, (p!)^2} = \sum_{p=0}^{n-j} \frac{(1 - m)_p\, (-n + j)_p}{(1)p} \frac{(1)^p}{p!}$$

$$= F(1 - m, -n + j; 1; 1)$$

$$= \frac{\Gamma(m + n - j)}{\Gamma(m)\, \Gamma(n - j + 1)}\,, \tag{C-7}$$

and substituting this expression into (C-6) gives the final result

$$\langle I^n \rangle = \left(\frac{b}{m}\right)^n \sum_{j=0}^{n} \binom{n}{j}^2 \frac{\Gamma(M + j)\,\Gamma(m + n - j)}{\Gamma(M)\Gamma(m)} \left(\frac{rm}{M}\right)^j \quad . \tag{C-8}$$

APPENDIX D

Reprinted from **APPLIED OPTICS**, Vol. 17, page 1786, June 1, 1978

Modeling solar cells for use as optical detectors: background illumination effects

Leo A. Mallette and Ronald L. Phillips

Solar cells have traditionally been used for direct sunlight to energy conversion, but there has been relatively little investigation into their use as a low data rate optical detector. This paper presents an experimental procedure used to determine the ac model of a specific solar cell. A lumped circuit model and governing equations are developed. Open circuit responses to pulses are used to determine values for the internal capacitances as a function of background illumination. Possible problems encountered with noise generation are also reviewed.

Introduction

List of Symbols

I	terminal current into solar cell,
I_λ	light generated current internal to cell,
k_d	constant coefficient associated with C_d,
k_j	constant coefficient associated with C_j,
V	terminal voltage of cell,
V_{bi}	diffusion or built-in potential,
τ_d	time constant associated with both C_d and C_j,
τ_j	time constant associated with C_j, and
τ_p	lifetime of minority carriers.

General

The photovoltaic effect was first observed by Becquerel in 1839, and over 100 yr later, it was observed by Ohl in a silicon p–n junction.[1] Modern manufacturing techniques have made low-cost silicon solar cells readily available. Availability of the material and price have prompted investigation into their use in areas other than direct sunlight to energy conversion; however, the feasibility of using a solar cell as a low data rate optical detector has been investigated by relatively few researchers.[2,3] In order to predict the response of a solar cell, the transfer function or the equivalent circuit must be known. In this paper an earlier model[3] is assumed, the individual elements are explained, the governing equations are given, and a method to fit numbers to the equations is developed. This paper assumes a constant temperature of 300 K; variation with temperature will be presented in a later paper.

Model

A solar cell is a p–n junction with part of its surface exposed to the environment. A diode and current generator in parallel can be used as a rough approximation for a solar cell model. All diodes have an inherent series resistance R_S and shunt resistance R_{SH},[2] and incorporating these yields an excellent approximation to the dc model of the solar cell. The cell current is proportional to the incident power by the spectral responsivity constant $R_{I\lambda}$[3] and is given by[4]

$$I = -I_\lambda + I_0\{\exp[-q(V - IR_S)/\eta kT] - 1\} + (V - IR_S)/R_{SH} \quad \text{(amperes)}. \tag{1}$$

For practical purposes, Shirland[4] defined R_S and R_{SH} in terms of the solar cell volt–ampere (V–I) characteristics as follows:

R_S is the reciprocal of the slope of the V–I curve at $I = 0$ (amperes). (2)

R_{SH} is the reciprocal of the slope of the V–I curve at $V = 0$ (volts). (3)

The remaining unknown element in the model (Fig. 1) is the diode, which can be characterized by three terms: (a) the junction resistance r, (b) the junction capacitance C_j, and (c) the diffusion capacitance C_d.

The junction resistance, usually called the dynamic resistance, is defined as the reciprocal of the slope of the V–I curve and is given by[5]

$$r = \frac{\eta kT}{qI_0}\exp(-qV_D/\eta kT) \quad \text{(ohms)}. \tag{4}$$

The authors are with Florida Technological University, Department of Electrical Engineering and Communication Sciences, Orlando, Florida 32816.

Received 1 October 1977.
0003-6935/78/0601-1786$0.50/0.

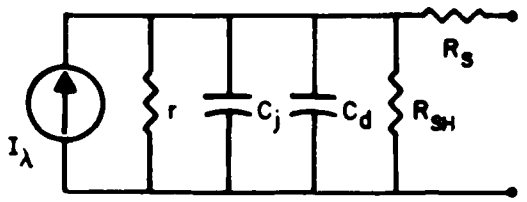

Fig. 1. Transient (ac) model of a solar cell.

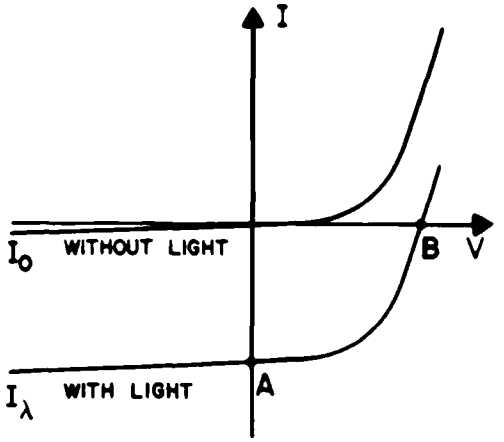

Fig. 2. Volt-ampere characteristics for photovoltaic cell with and without background illumination.

The junction capacitance is defined[6] as the incremental charge increase dq of fixed, unneutralized donors or acceptors per incremental voltage change dv and is given by[5,7,8]

$$C_j = k_j/(V_{bi} - V_D)^{1/2} \quad \text{(farads)}. \tag{5}$$

The diffusion capacitance term C_d is a result of the photoinjected electron-hole pairs. On either side of the junction, pairs of majority and minority carriers are generated whenever a photon is absorbed. The addition of majority carriers is negligible, but there is a highly noticeable increase in the percentage of minority carriers. These carriers will either recombine with majority carriers or diffuse to the junction and drift to the opposite side of the junction where they become majority carriers. The lifetime of the minority carrier is defined as τ_p,[6] and the diffusion capacitance can be shown to be[8]

$$C_d = \tau_p/r \quad \text{(farads)}, \tag{6}$$

where r is defined by Eq. (4).

Since τ_p is a constant, C_d can be shown to be[8]

$$C_d = k_d \exp(\alpha V_D) \quad \text{(farads)}. \tag{7}$$

Experimental Procedure

Resistances

Two V-I characteristics of the solar cell, shown in Fig. 2, are measured using a commercially available curve tracer. The reciprocal of the slope of the V-I curve, measured in the presence of background light and evaluated at points A (I-axis intercept) and B (V-axis intercept), yields the shunt and series resistances, respectively.[4] This curve is similar to the no-light curve, but translated down by $I_\lambda - (V - IR_S)/R_{SH}$ amperes, and translated to the right by IR_S volts. Note: these V-I characteristics are for the entire solar cell and not for the internal diode.

The internal diode current and voltage are given by[3]

$$V_D = V - IR_S \quad \text{(volts)}, \tag{8}$$

and

$$I_D = I - (V - IR_S)/R_{SH} \quad \text{(amperes)} \tag{9}$$

The data points of the V-I curve can be corrected using Eqs. (8) and (9) to supply the $V_D - I_D$ curve of the diode. These corrected data points are fitted to the equation[3]

$$I_D = I_0(\exp(\alpha V_D) - 1) \quad \text{(amperes)} \tag{10}$$

The dynamic resistance r is obtained by taking the reciprocal of the derivative of Eq. (10), or via Eq. (4), noting that α of Eq. (10) is $q/\eta kT$.

Junction Capacitance

Saltsman[3] used the circuit of Fig. 3 to determine the junction capacitance by measuring the impulse response of the cell for various values of dc bias. The bias resistor R_B was chosen so that $R_S \ll R_B \ll R_{SH}$. R_C and C_C were chosen to provide ac coupling, to keep the peak value of the impulse small, and to have a long time constant. The cell voltage V, as observed on an oscilloscope, is a decaying exponential superposed on the dc bias, which is generated by the background illumination. The decay time constant τ_j will vary as a function of temperature and background illumination. The decay time constant is given by[3]

$$\tau_j \cong R_B C_j \quad \text{(sec)} \tag{11}$$

The decay time constant can be determined from the cell voltage V as observed on an oscilloscope.

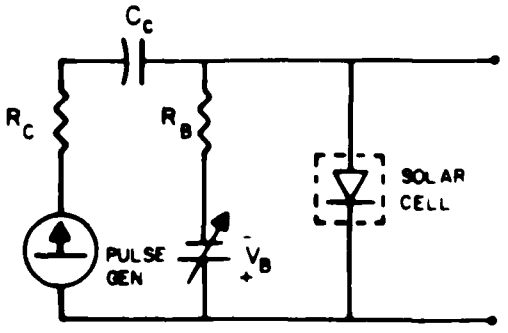

Fig. 3. Test circuit used to determine junction capacitance of the solar cell.

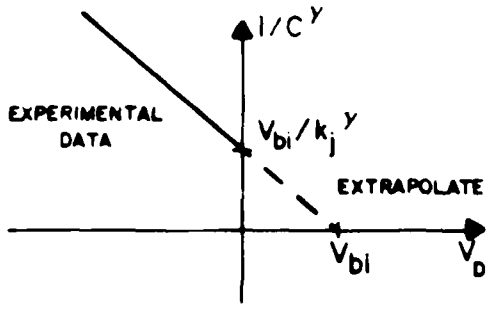

Fig. 4. Method to determine built-in voltage V_{bi} and constant k_j.

Dividing τ_j by R_B yields the junction capacitance for various values of reverse bias voltage. These values of capacitance must be fitted to Eq. (5). One method is to assume a value for γ and plot the experimental data points as shown in Fig. 4. If the value for γ was correctly chosen, the points will form a straight line; otherwise, a different value of γ must be chosen.[9] The line connecting the experimentally measured points may be extended to the V_D axis. The built-in potential can be read off the graph, since the V_D-axis intercept is at $(V_{bi} - V_D) = 0$. Similarly, the constant coefficient k_j can be determined from the $1/C^{\gamma}$-axis intercept.

Diffusion Capacitance

The authors developed a method[8] to determine the diffusion capacitance using a narrow-pulse laser and a source of controllable background illumination. The background illumination generates a dc current I_λ and hence a voltage V_D across the diode. The two lasers[10] coimpinged on the face of the solar cell, and the open circuit decay time constant was measured as well as the dc output voltage. The magnitude of the pulse had to be kept small, compared with the background illumination, in order that it not significantly perturb the cell by itself. Due to background illumination, the time constant will be a function of both the junction capacitance and the diffusion capacitance, and it is given by

$$\tau_d = \left[\frac{1}{(R_S + R_L)} + \frac{1}{R_{SH}} + \frac{1}{r}\right](C_j + C_d) \quad \text{(sec)}. \qquad (12)$$

The $1/(R_S + R_L)$ term is negligible because of the method of open circuit measurement (coupling directly to an oscilloscope). The other terms in Eq. (12) have been previously determined and are either constants or functions of V_D.[11] A graph of τ_d vs output voltage will yield a family of monotonically decreasing functions from $V = 0$ volts to $V \cong V_{bi}$. The junction capacitance dominates at the lower voltages, and (as shown below) noise dominates at the higher voltages. Since k_d is the only unknown in Eq. (12), one point will uniquely determine its value. Theoretically this is sufficient, but the authors have found that fitting an entire set of measurements will eliminate random errors.

Noise Generation

Because of internal resistance, physical size, exposure to the environment, and the quantum mechanism of operation, solar cells are subject to nearly every known noise identified to date! In considering the SNR, six noises the reader should be aware of are[5,12]

(a) Johnson noise. Also called Nyquist, resistance, or thermal noise.

(b) Temperature noise shifts the spectral response toward the ir as temperature increases.

(c) Modulation noise. Also called excess or $1/f$ noise.

(d) Generation–recombination (G–R) noise. The variation can be caused by the random arrival of photons from the background illumination. For this case, the noise is also called photon, radiation, or background noise.

(e) Shot noise is due to the discrete nature of the current. The total current of the unbiased cell is comprised of minute current pulses produced by the individual electron-hole pairs being generated. This noise was intense when the cell was exposed to high levels of background illumination.

(f) 60-Hz noise is the modulation of the background illumination by 60 Hz and its harmonics.

Summary

A general model for a solar cell was developed using lumped resistors and capacitors. The resistances are determined from the V–I characteristics of the cell. The junction and diffusion capacitances are determined by observing the decay time constant of electrical and optical impulses, respectively. The method should be applied in the same chronological order as this paper, isolating the ac and optical effects, then releasing the ac isolation requirement to measure the junction capacitance, and finally the optical isolation requirement to calculate the diffusion capacitance. Changing the background illumination will cause significant variation in the value of τ and hence may wreak havoc on any form of digital signal processing equipment in the detection system.

The authors thank W. A. Kownacki for his many valuable suggestions. Funding for this project was provided by the U.S. Army project manager for training devices.

References

1 U.S. Patent 2,402,662, filed 27 May 1941.
2 P. G. Witherell and M. E. Faulhaber, Appl. Opt. 9, 733 (1970).
3 S. O. Saltsman, *The Silicon Solar Cell as an Optical Detector* (Florida Technological U., Orlando, 1977).
4 F. A. Shirland, *Solar Cells* (IEEE, New York, 1976), p. 43.
5 J. Millman and C. C. Halkias, *Integrated Electronics: Analog and Digital Circuits and Systems* (McGraw-Hill, New York, 1972).
6 D. H. Navon, *Electronic Materials and Devices* (Houghton Mifflin, Boston, 1975).
7 S. M. Sze, *Physics of Semiconductor Devices* (Wiley, New York, 1969).
8 L. A. Mallette, *Modeling the Silicon Solar Cell as an Optical Detector* (Florida Technological U., Orlando, 1977).
9 R. P. Nanavati, *Semiconductor Devices* (Intext, New York, 1975).
10 In our case, we used a 750 mW Ar ion laser manufactured by Control Laser Inc., Orlando, Fla., as a source of background illumination.
11 For open circuit measurements, there is no current flow in R_S and no voltage across it; therefore, $V = V_D$.
12 U.S. Department of the Navy, Office of Naval Research, *Handbook of Military Infrared Technology* (GPO, Washington, D.C., 1965).